AN INVESTIGATION OF GROUND EFFECT ON VERTICAL TAKEOFF AIRCRAFT

Charles Douglas Thompson

United States
Naval Postgraduate School

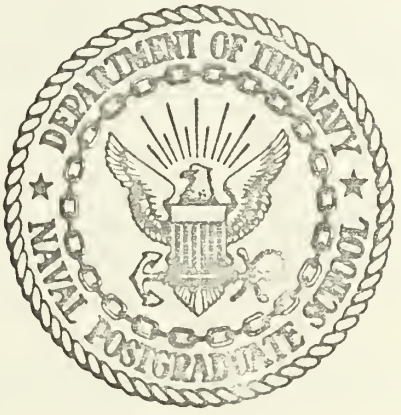

THESIS

AN INVESTIGATION OF GROUND EFFECT
ON VERTICAL TAKEOFF AIRCRAFT

by

Charles Douglas Thompson

June 1970

An Investigation of Ground Effect on Vertical Takeoff Aircraft

by

Charles Douglas Thompson
Lieutenant (junior grade), United States Navy
B.S.M.E., University of Mississippi, 1969

Submitted in partial fulfillment of the
requirements for the degree of

MASTER OF SCIENCE IN MECHANICAL ENGINEERING

from the

NAVAL POSTGRADUATE SCHOOL
June 1970

ABSTRACT

The theoretical solution for the flow beneath V/STOL aircraft was extended to include tilted jet configurations. A laboratory model was constructed to test the effect of variation of the parameters governing the flow. Free streamline plots, pressure coefficients on the ground and fuselage and velocity profiles in the nozzles were determined from hot-wire anemometer traverses and micromanometer readings. Experimental data compared favorably with the theoretical determinations.

TABLE OF CONTENTS

I. INTRODUCTION 9

II. OBJECT 11

III. THEORY 12

IV. COMPUTER ANALYSIS 16

V. DESIGN CONSIDERATIONS 19

VI. PROCEDURE 23

VII. RESULTS 25

VIII. DISCUSSION OF RESULTS 48

IX. CONCLUSIONS 50

X. RECOMMENDATIONS 51

APPENDIX A 52

COMPUTER PROGRAM 58

BIBLIOGRAPHY 73

INITIAL DISTRIBUTION LIST 74

FORM DD 1473 75

SYMBOLS

A	a constant
C_p	pressure coefficient
I	flow region in the ζ plane
K	complete elliptic integral of the first kind
K'	defined by $K'(k) \equiv K(k')$
k	modulus of elliptic integral
k'	defined as $\sqrt{1 - k^2}$
p	pressure
p_o	ambient pressure outside jets
Q	an angle used to evaluate Ω functions
R_e	Reynolds number, $\Delta V_o/\nu$
T	complex variable in T-plane, $\xi + i\eta$
t	complex variable in t-plane
u	velocity in x-direction
V	velocity
V_I	velocity at nozzle exit
$\overline{V}_I$	average velocity at nozzle exit
V_o	velocity along free streamlines
v	velocity in y-direction
W	complex potential, $\Phi + i\psi$
x,y	coordinates in physical plane
z	complex variable, $x + iy$
α	tilt angle of nozzle
β	plate angle
Γ	flow region in the T-plane

Δ	width of nozzle
δ_L, δ_R	asymptotic widths of streams flowing to left and to right
ζ	complex conjugate velocity, u-iv
θ	Theta-function
Θ	function defined in equation (4)
ξ,η	coordinates of T-plane
ρ	density
Φ	velocity potential
ψ	stream function
Ω	function defined in Appendix A

Subscripts:

A,G,H	refer to stagnation points
r	refers to boundary point

ACKNOWLEDGEMENTS

I am particularly indebted to Assistant Professor T. M. Houlihan for his invaluable guidance and assistance through all phases of this research. Assistant Professor R. H. Nunn's comments and corrections to the rough draft are also greatly appreciated. I should also like to acknowledge the aid of Mr. Ken Mothersell who patiently helped me with the practical design and construction of the test equipment.

I. INTRODUCTION

In recent years crowded airport facilities, the search for rapid urban transportation and the need for military aircraft capable of operating from advanced bases has resulted in a great deal of attention being given to V/STOL (vertical/short take-off and landing) aircraft. Much research has been performed on various models and full-scale versions of these aircraft. Some operational types have been developed.

When operating near the ground these aircraft are quite similar in principle to ground effect machines. Ground effect can be either beneficial or detrimental depending upon the configuration of the aircraft. Land erosion, damage to objects near the operating area and recirculation of debris and hot exhaust gases beneath the fuselage are some of the problems involved with hovering near the ground. The reingestion of exhaust gases reduces the efficiency of the engines. Recirculating debris may also enter the engines or severely damage the underside of the aircraft. Some pilots have experienced handling difficulties, drastic loss of power and visibility problems as a result of ground effect.

The recirculating flow underneath the aircraft, however, can also produce a lifting force which can significantly reduce the thrust necessary to operate the aircraft. Small modifications to the aircraft such as tilting of engines can often reduce the unfavorable effects to such an extent that the additional lift provided by the recirculating flow can produce improved performance. A mathematical model of the flow field beneath V/STOL aircraft would permit designers to estimate the effects of various modifications analytically.

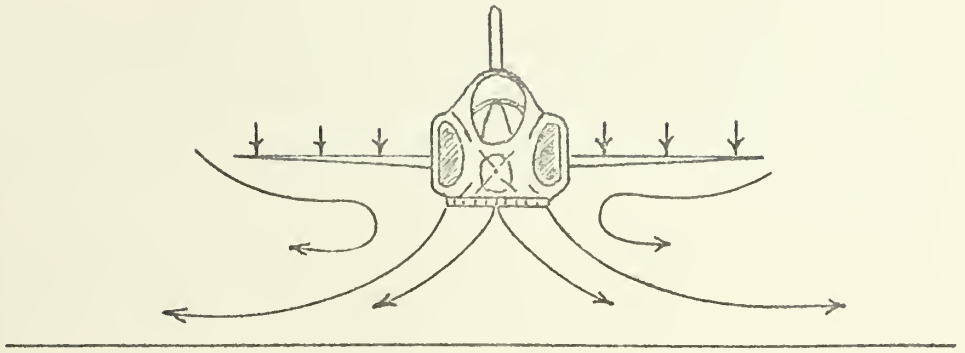

Unfavorable ground effect

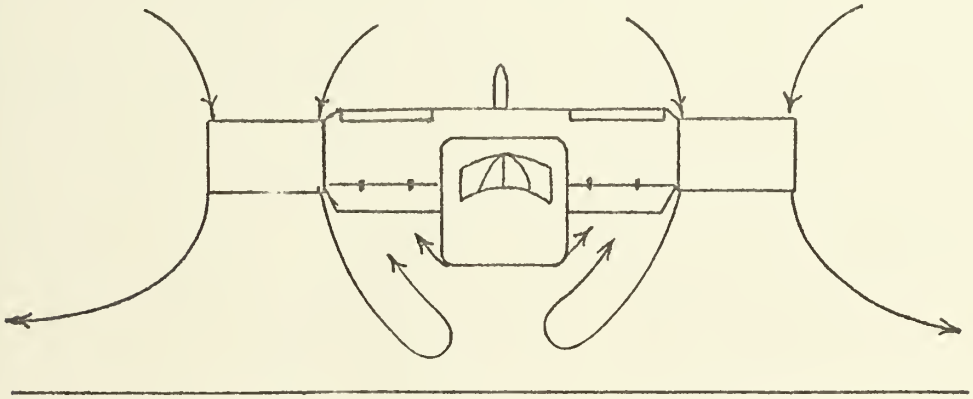

Favorable ground effect

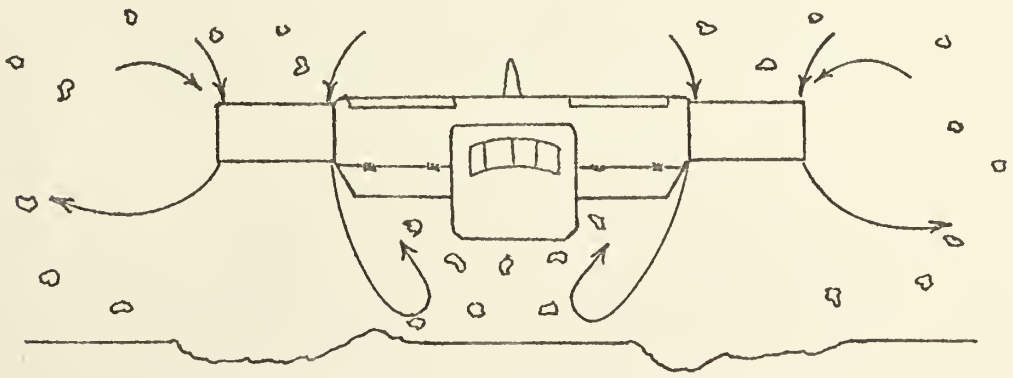

Surface erosion and debris recirculation

FIGURE 1

II. OBJECT

The theoretical solution for the flow field beneath V/STOL aircraft with two vertical two-dimensional jets has been presented in a series of three NASA reports. The purpose of this research was to obtain experimental verification of the present theory and to extend the theory to include other possible configurations.

III. THEORY

An analytical solution to the flow beneath a V/STOL aircraft was obtained by Goldstein and Siegel [Ref 3]. They considered a two-dimensional model of an aircraft with a slot jet exhaust or fan pod in each wing. The analysis was performed assuming an incompressible, inviscid, isothermal, irrotational, steady flow. A flat plate at an angle to the ground represented the fuselage. The flow field was mapped into a hodograph plane and a complex potential plane. A brief outline of this analysis is given in Appendix A.

So that entrainment could be ignored this solution assumed that the nozzles were within a few nozzle widths of each other. For the same reason the nozzles were also required to be within a few nozzle widths of the ground. The nozzles were assumed to be perpendicular to the ground. Since tilting of nozzles is one possible solution to recirculation problems, a more general analysis should allow the nozzles to be at some angle to the perpendicular.

Considering the flow field shown in Figure 2 and proceeding exactly as did Goldstein and Siegel the hodograph and complex potential planes are as shown in Figure 3-1 and 3-2. The function which maps the rectangular region Γ in the T-plane (figure 3-3) into the hodograph plane is

$$\zeta(T) = V_o \, e^{i(\pi/2-\alpha)} \, \Omega(T;\xi_H,k) \, \sqrt{\Omega(T;\xi_G,k)} \, [\Omega(T;\xi_A,k)]^{\beta/\pi} \qquad (1)$$

where the Ω function is as defined in Appendix A. Taking the argument of this function and requiring that the direction of the flow along the plate must equal the argument, it can be shown that

Physical flow field, 2-d tilted jets,
$z = x + iy$

FIGURE 2

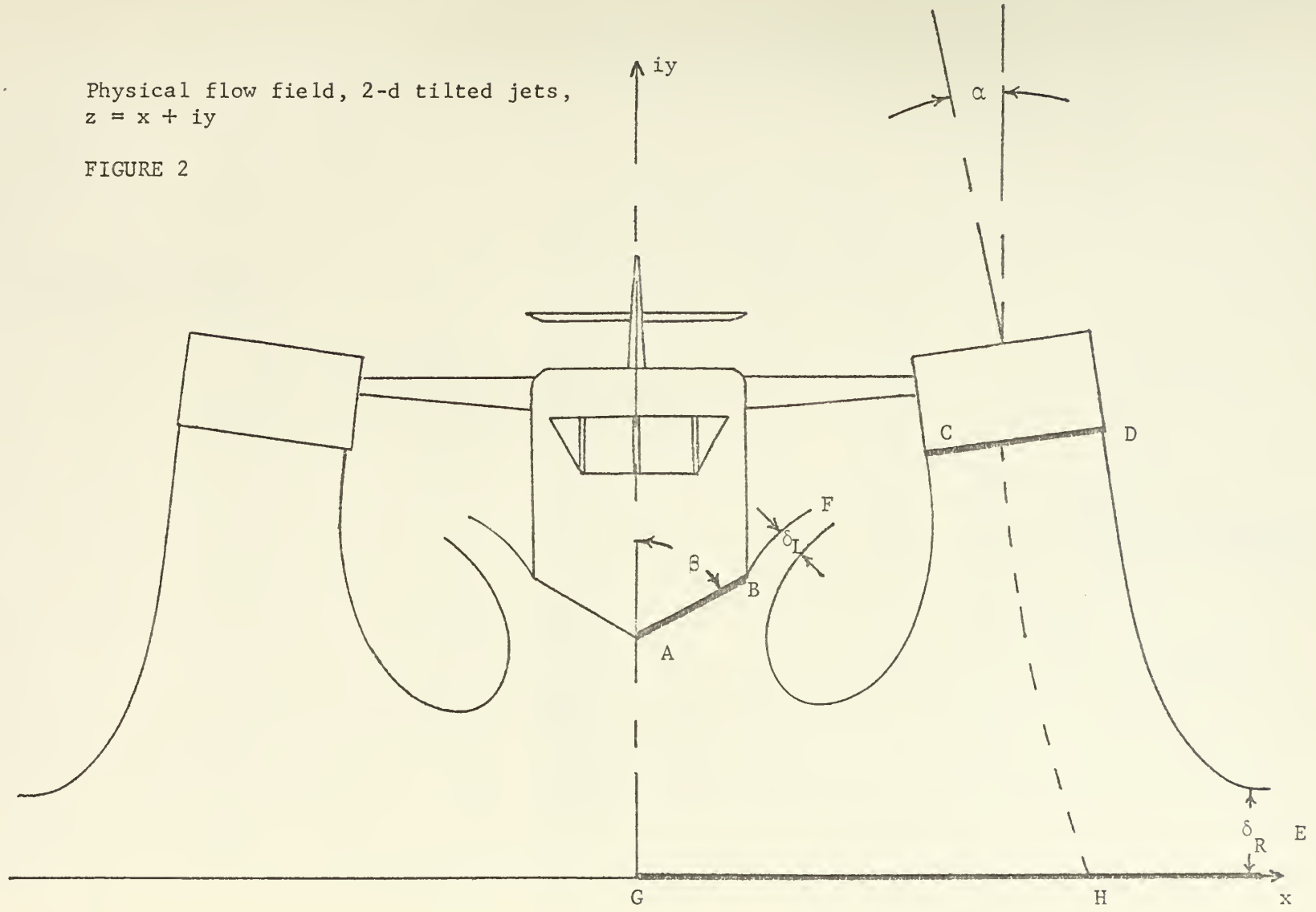

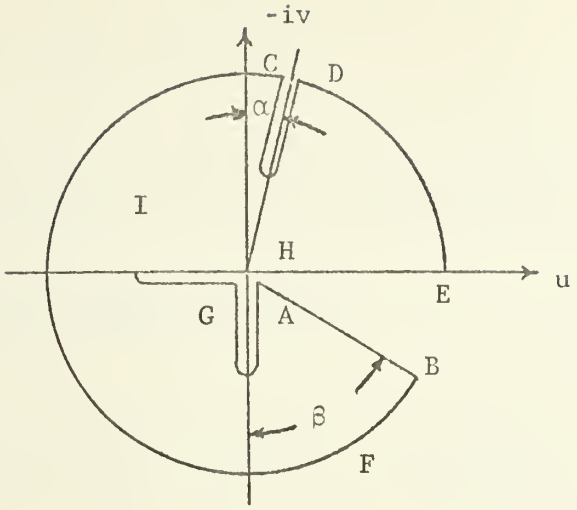

(1) Hodograph plane, $\zeta = u - iv$

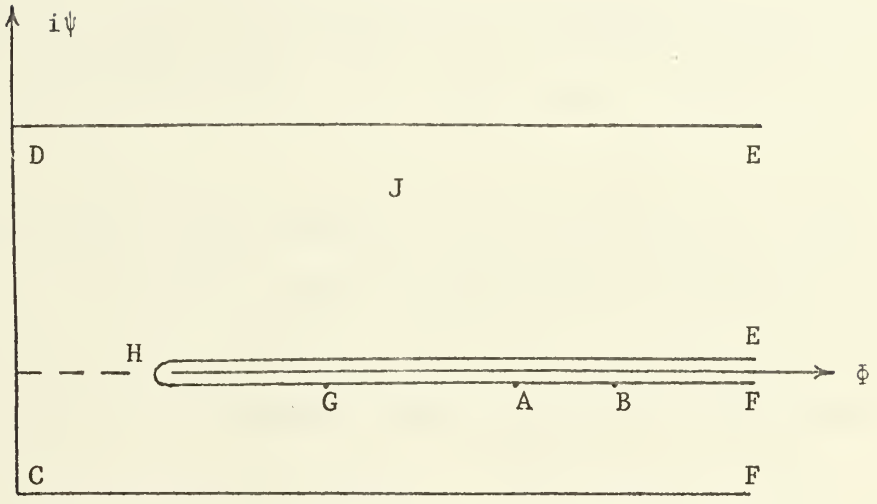

(2) Complex potential plane, $W = \Phi + i\psi$

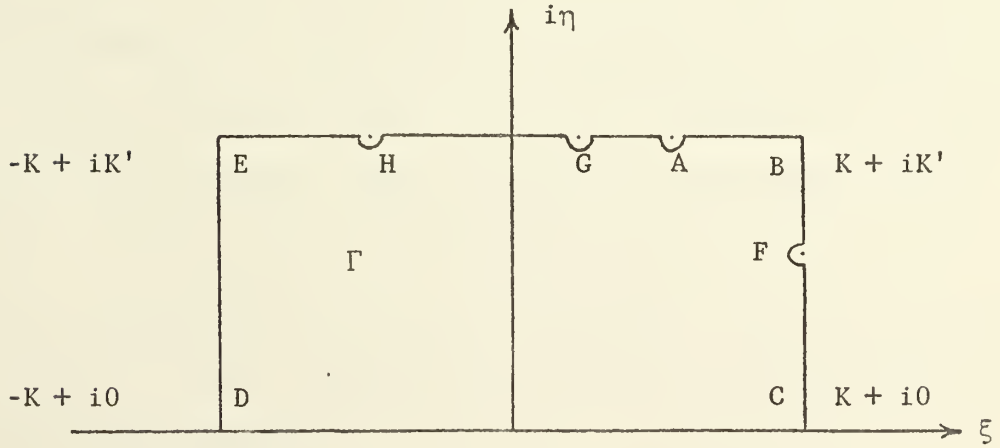

(3) T-plane

FIGURE 3

$$\frac{4K}{\pi}\left(\frac{\pi}{4}+\alpha+\frac{\beta}{2}\right)=2\xi_H+\xi_G+\frac{2\beta}{\pi}\xi_A \tag{2}$$

The remainder of the analysis proceeds exactly as before and the final solution for displacement in the flow field becomes

$$\frac{z}{\Delta}=\left(\frac{\bar{V}_I}{V_o}\right)e^{i\alpha}\frac{k'}{\pi}\left[\frac{sn\ (\eta_F,k')+\delta_R/\delta_L}{1+\delta_R/\delta_L}\right]$$

$$X\int_{\xi_G+iK'}^{T}\frac{(k\ sn\ \xi_H\ snT-1)\ (1-k\ snT)\ dT}{dnT[1-dn(\eta_F,k')\ snT]\ \Omega(T;\xi_H,k)\ \sqrt{\Omega(T;\xi_G,k)}\ [\Omega(T;\xi_A,k)]^{\beta/\pi}} \tag{3}$$

There are in this case six parameters which determine the flow field: plate height, plate width, plate angle, nozzle height, nozzle spacing and nozzle angle.

The plate and nozzle angles appear in the solution but the other parameters must be calculated. Following the example of Goldstein and Siegel the solution is determined by integrating along the sides of the rectangular region Γ in the counterclockwise direction. Thus the distance between two points in the physical plane is the difference between the line integral from the point G in the T-plane (origin in the physical plane) to each of the points in question. If all distances are non-dimensionalized by the nozzle width the solution can be obtained using the known plate and nozzle angles and the four following input parameters: k, δ_L/δ_R, η_F/K'. and ξ_A/K. These parameters all have values ranging between zero and one, but no representative values were given in Ref. 3. Upon direct communication with the Lewis Research Center it was learned that no values of these parameters and their corresponding physical configurations were available.

IV. COMPUTER ANALYSIS

Using the working formulas in the appendixes of Refs. 3 and 4, two computer programs were written. The first program calculated the plate height and width and nozzle height and spacing for a given set of input parameters. The second program was merely a variation and extension of the first. For a given set of input parameters and experimental data the second program plotted the theoretical flow field, the pressure coefficients on the ground and plate and the velocity profile in the nozzles along with the data points. A copy of the second program follows Appendix A.

The plate and nozzle angles were read from data cards. In the second program the input parameters were also read from cards, but in the first program the parameters were initialized and iterated in steps of one tenth. The complete elliptic integral of the first kind, the complimentary modulus and the complimentary integral were all calculated from k. The various quantities and functions were then evaluated as indicated in the program.

The modified equation for ξ_G is equation (2) of this thesis. The modified equation for Θ is

$$\Theta^{(i)}(\eta) = \frac{\pi}{2} - \alpha + Q_H^{(i)}(\eta) + \frac{1}{2} Q_G^{(i)}(\eta) + \frac{\beta}{\pi} Q_A^{(i)}(\eta) \quad i = 3,4 \qquad (4)$$

These modifications provide for solutions with the nozzles tilted. The $Q_r^{(i)}$'s are angles defined in Ref. 4. It should be pointed out that $Q_r^{(3)}$ must be taken as a negative angle in the third or fourth quadrant, while $Q_r^{(4)}$ must be taken as a positive angle in the first or second quadrant.

The height and width of the plate were calculated directly by integration. The nozzle spacing was found by first locating the point B at

the end of the plate and then adding to that the horizontal separation of the points B and C. The nozzle height was found similarly by adding the vertical separation of the points D and E to the width of the flow to the right.

At this point the values calculated were printed out. In the first program the parameters were iterated here and a new configuration was calculated. In the second program plotting was begun at this point.

The data points were plotted first and then the theoretical free streamlines were plotted. A similar procedure was followed for the pressure coefficients and the nozzle exit velocity. The velocity was made negative to fix the direction downward, so that the plotted profile was as if it were being viewed from in front of the aircraft.

All integrations were performed by the Gauss nine-point quadrature formula. When infinite series were specified only the first five terms were taken. In the working formulas presented in Ref. 3 quite often square roots and odd powers were taken of the negatives of numbers. On the intervals indicated this would be quite proper since the numbers would be negative values before having the sign changed. Since the programs were to be used to find possible combinations of the input parameters, quite often, if the parameters were wrong, the result would be an attempt to take the logarithm or square root of a negative number. To prevent the computer from ending the calculation with error messages, absolute values were taken of all functions under radicals. This was equivalent to the operation intended in the original notation, but avoided the problems in calculation.

In the first program statements were included in all the functions to notify the operator if a denominator was zero. The second program

has retained the check on the denominator and sets the function to a nominal value of one thousand in the event the denominators are very small. This is intended only to avoid underflow errors at the limits of the integration; no notification is given to the operator in this case. The second program is therefore intended to be used only with combinations of the parameters which are known to satisfy all the equations.

V. DESIGN CONSIDERATIONS

A model of a V/STOL aircraft using two-dimensional slot jets in an inviscid, incompressible fluid was required to verify the theoretical results. The test apparatus was designed to approximate these conditions as closely as possible.

Air at low pressure was used to represent the incompressible, inviscid fluid. The two-dimensional slot jets were produced by two rectangular nozzles with a cross-sectional width to length ratio of four to one. By confining all measurements to a plane through the centers of the two nozzles, end effects could be ignored.

To avoid entrainment problems the theory required that the nozzle half-spacing and height be only a few jet widths. This condition suggested the use of a large nozzle width so that there would be enough room to probe the flow field beneath and between the nozzles. Also to permit a significant number of data points for plates with half widths as small as one fourth of a jet width, a large nozzle width was required. The test apparatus was designed with nozzles two inches wide.

Even with low nozzle exit velocities a large flow rate was necessary to supply the system. Thus, the nozzles were connected to the laboratory turbine compressor. Each nozzle was attached to the air supply through a flow straightening, diffuser chamber. Rotameters preceded these chambers in the air lines. Thus, air flow conditions could be monitored easily throughout the test period. As air entered the diffuser chamber it was deflected by three layers of wire screen. The air then passed through a layer of honeycomb material into the nozzle, thus producing a uniform velocity distribution throughout the nozzle.

Laboratory model of V/STOL aircraft using
symmetrical two-dimensional slot jets

FIGURE 4

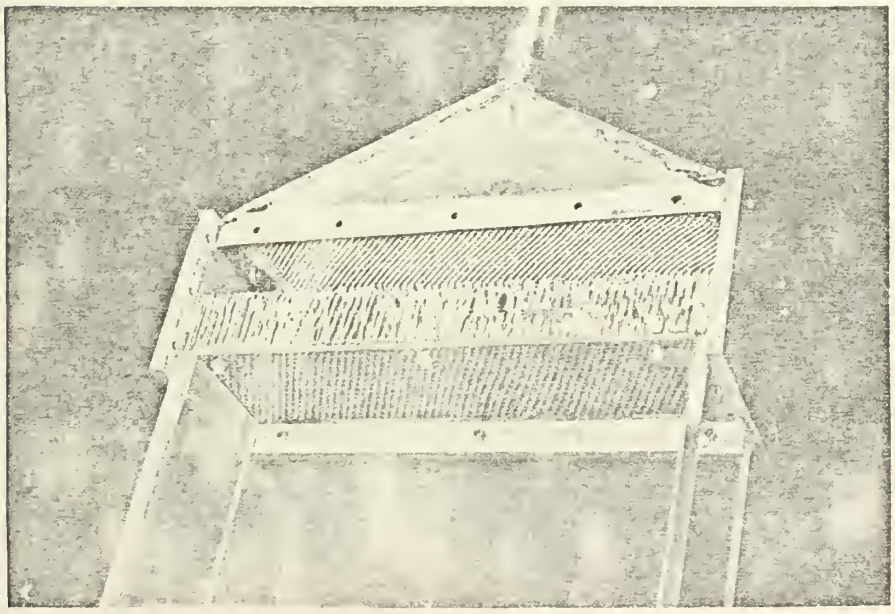

Flow straightening chamber

FIGURE 5

The flow straightening sections also served as a mounting for the nozzles. If desired, the nozzle shape and size could be changed quite easily.

A mounting arrangement was designed to not only allow the nozzles to be moved vertically and horizontally but also to be rotated in the vertical plane, thereby representing a tilted jet configuration. This freedom of movement was accomplished by connecting the flow straightening section to a vertical rod through a swivel which could be locked at any angle. The vertical rod passed freely through a metal block, and it too could be locked in any position. The block moved horizontally along parallel bars and could be held firmly in position with a set screw. The parallel bars were mounted in a rigid framework which was supported by four legs.

Directly underneath the framework and the nozzles was a large plexiglass plate which represented the ground. Smaller plates representing fuselages of various sizes and shapes were made to be interchangeable on a bracket which was suspended from the framework between the nozzles. The vertical position of the plate bracket was varied with a threaded traverse. The ground plate and the fuselage plates contained a row of pressure taps across the center section. For future studies with smaller nozzles and higher velocities, significant pressure measurements would be made possible, but for these low velocity tests the primary measurements were made with a hot-wire anemometer.

To support the hot-wire probe a traversing mechanism was mounted on the apparatus. The mechanism allowed the probe to be held at a constant depth into the flow while traveling both horizontally and vertically throughout the field.

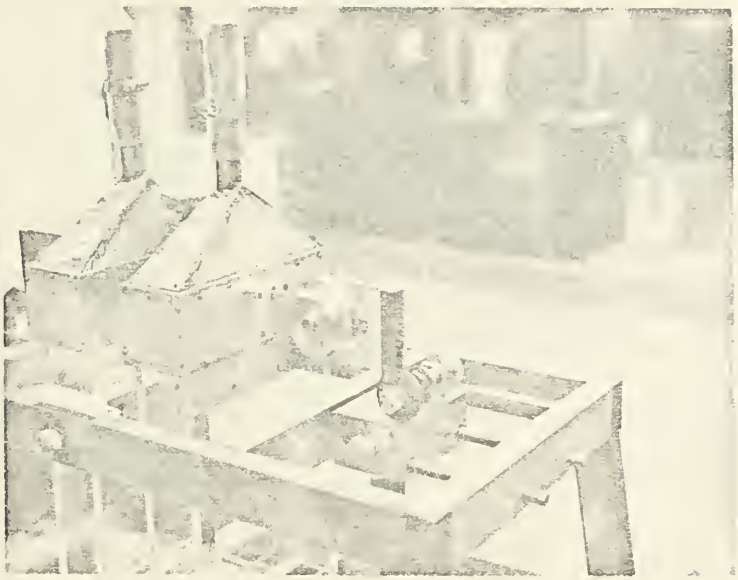

Nozzle mounting arrangement

FIGURE 7

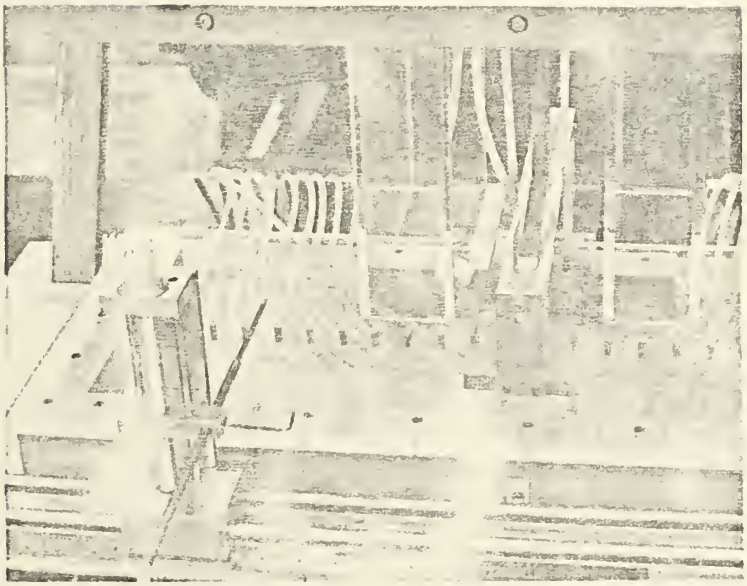

Traversing mechanism

FIGURE 8

VI. PROCEDURE

A list of plate heights and widths and nozzle heights and spacings for which the corresponding input parameters were known was compiled. From this list a few representative configurations were chosen for experimental verification.

The plate size, height and angle and nozzle spacing, height and angle were all set and recorded. The compressor was then started and an equal air flow was routed to each nozzle through the flow meters. A straight hot-wire probe was placed under one edge of one of the nozzles. The voltage and location was recorded. Then by following the motion of a fine thread placed in the flow field, the probe was moved horizontally in convenient intervals and then moved vertically until the same voltage was again observed. Since only velocity magnitudes were of interest, the probe was always rotated to obtain a maximum reading. By following this procedure from both sides of a nozzle and from the edge of the upper plate the coordinates of the lines of constant voltage (free streamlines) could be recorded.

The probe was then moved as close to the upper plate as possible and oriented to read the velocity in the direction of the plate. By moving the probe in convenient intervals along the plate the velocity distribution along the plate could be recorded. Similarily the probe was moved along the lower plate and the voltage and horizontal position were recorded.

This procedure was followed with each configuration. Tests were run with Reynolds numbers varying from 1600 to 7000. Simultaneously pressure measurements were made using a micromanometer capable of indicating

pressures as low as .001 inches of water. The pressure and location were recorded for comparison with the hot-wire data.

The data collected in this manner was sufficient to plot the free streamlines of the flow field, the nozzle exit velocity profile and the pressure coefficient along the plate and ground. The input parameters for each configuration were read into the program along with the experimental data. The experimental results for each configuration were then plotted along with the corresponding theoretical results.

VII. RESULTS

The results of the experiments are presented in the following pages. Table I is a list of some of the input parameters for which the corresponding configurations were found.

Figures 8-1 through 12-1 are typical free streamline plots for various configurations. Hot-wire data points are represented by triangles. The coordinates are nondimensionalized with the nozzle width.

The pressure coefficient along the ground is shown in Figures 8-2 to 12-2. Only the abscissa is nondimensionalized. The pluses represent data points calculated from manometer readings.

The pressure coefficient on the plate is shown in Figures 8-3 through 12-3. Again, only the abscissa is nondimensionalized.

Figures 8-4 through 12-4 are the plots of the nozzle exit velocity profile. The velocity is nondimensionalized with respect to the maximum velocity recorded for that test. The abscissa is one nozzle width in length. The velocity is plotted negatively so that the plot represents the actual direction of the flow.

Figures 13 and 14 clearly indicate the nature of the flow field beneath the nozzles.

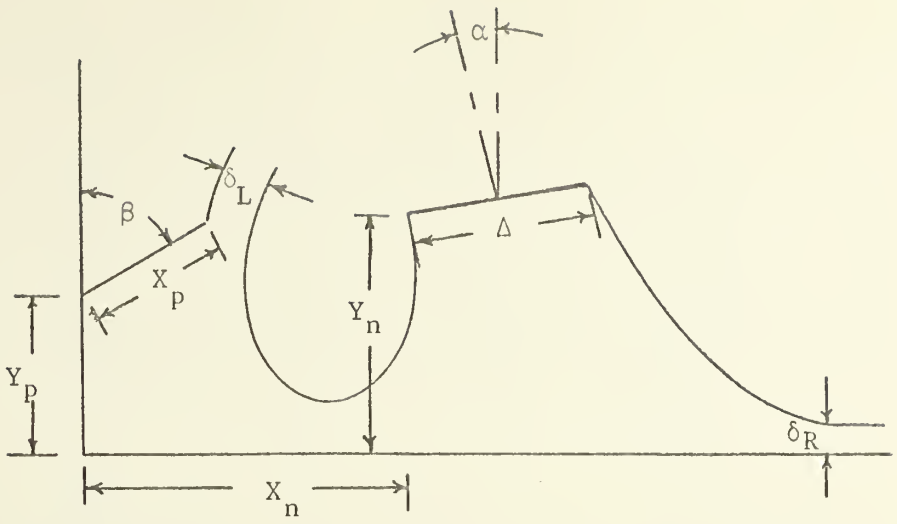

K	$\frac{\delta_L}{\delta_R}$	$\frac{\eta_F}{K'}$	$\frac{\xi_A}{K}$	β	α	$\frac{X_p}{\Delta}$	$\frac{Y_p}{\Delta}$	$\frac{X_n}{\Delta}$	$\frac{Y_n}{\Delta}$
.2	.4	.6	.1	90	0	.551	.886	.798	1.61
.3	.1	.9	.4	90	0	1.12	1.34	1.29	1.57
.3	.1	.9	.5	90	0	.594	1.34	.769	1.58
.3	.2	.7	.3	90	0	.692	.966	1.01	1.48
.3	.3	.6	.2	90	0	.559	.860	.725	1.43
.3	.3	.7	.5	90	0	.405	.772	.775	1.35
.4	.1	.9	.5	90	0	.593	1.23	.741	1.37
.4	.2	.7	.4	90	0	.576	.874	.826	1.26
.4	.5	.7	.7	90	0	.309	.449	.719	1.05
.5	.1	.7	.2	90	0	.802	1.00	.962	1.27
.6	.1	.7	.3	90	0	.646	.879	.760	1.07
.6	.1	.8	.4	90	0	.698	.917	.696	1.04
.3	.2	.7	.4	90	10	.547	.722	.824	1.26
.5	.1	.7	.3	90	10	.687	.787	.831	1.07
.3	.2	.7	.2	60	0	.478	.770	.736	1.53
.5	.1	.7	.1	60	0	.502	.827	.601	1.36
.3	.1	.9	.5	60	10	.422	.863	.460	1.40
.5	.1	.7	.2	60	10	.441	.617	.527	1.12
.3	.1	.9	.2	45	0	.879	.715	.747	1.63
.4	.2	.9	.4	45	0	.851	.520	.718	1.27

TABLE I

Input parameters and corresponding configurations

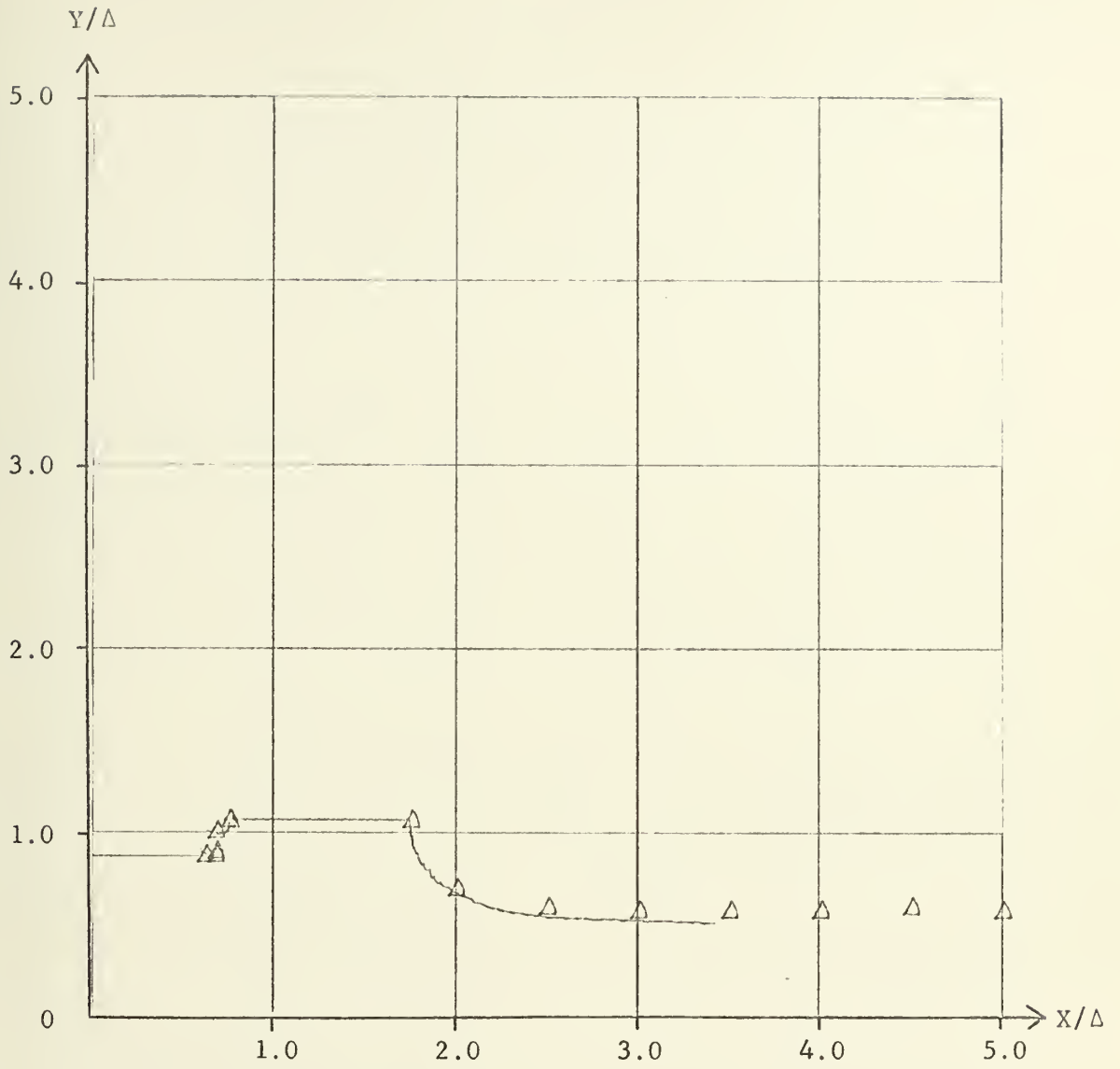

$\frac{X_p}{\Delta} \approx .65$ $\frac{Y_p}{\Delta} \approx .88$ $\frac{X_n}{\Delta} \approx .76$ $\frac{Y_n}{\Delta} \approx 1.1$

$\beta = 90$ $\alpha = 0$

$Re \approx 6200$

FIGURE 8-1 Free streamline plot

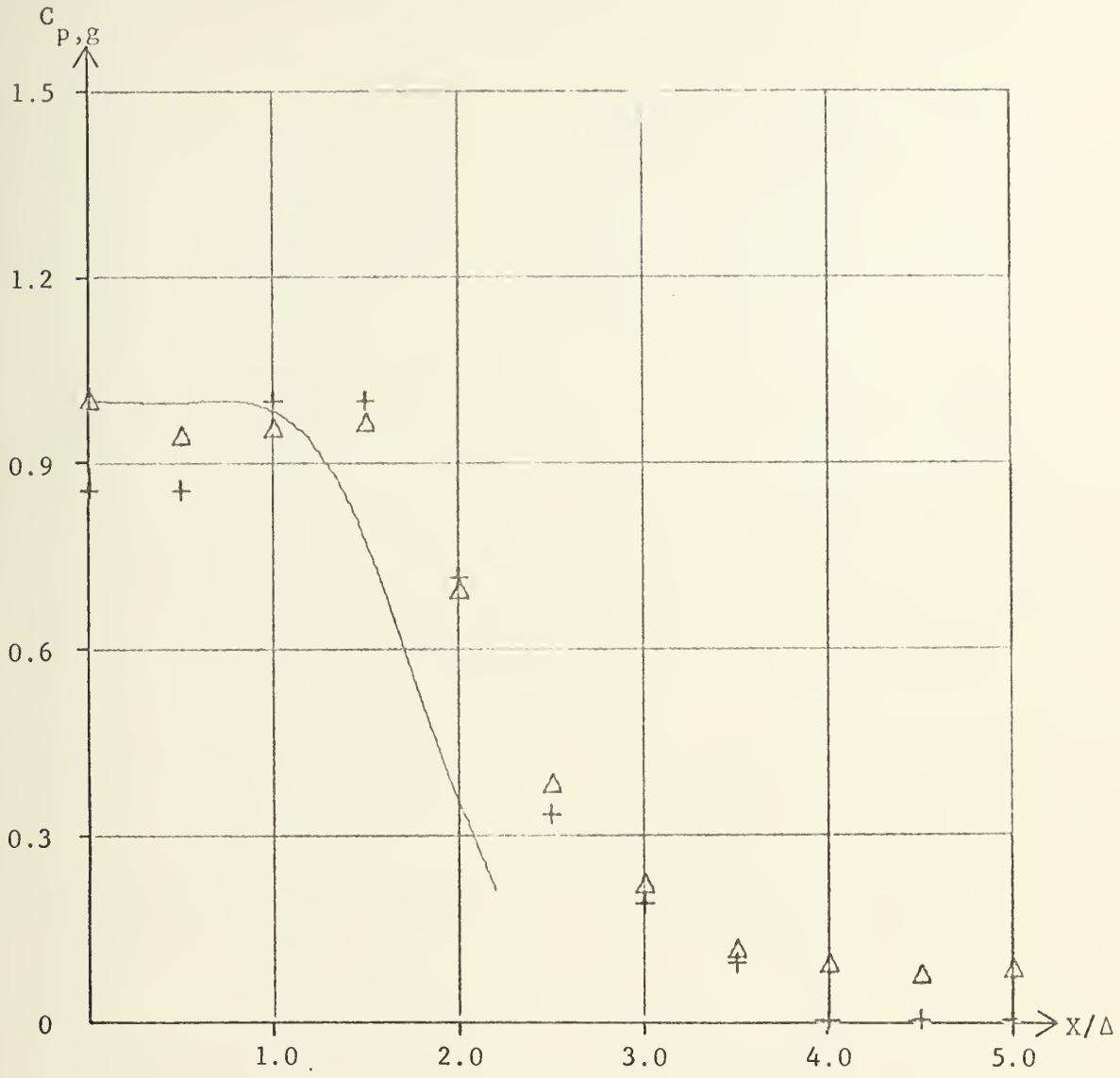

FIGURE 8-2 Pressure coefficient along the ground

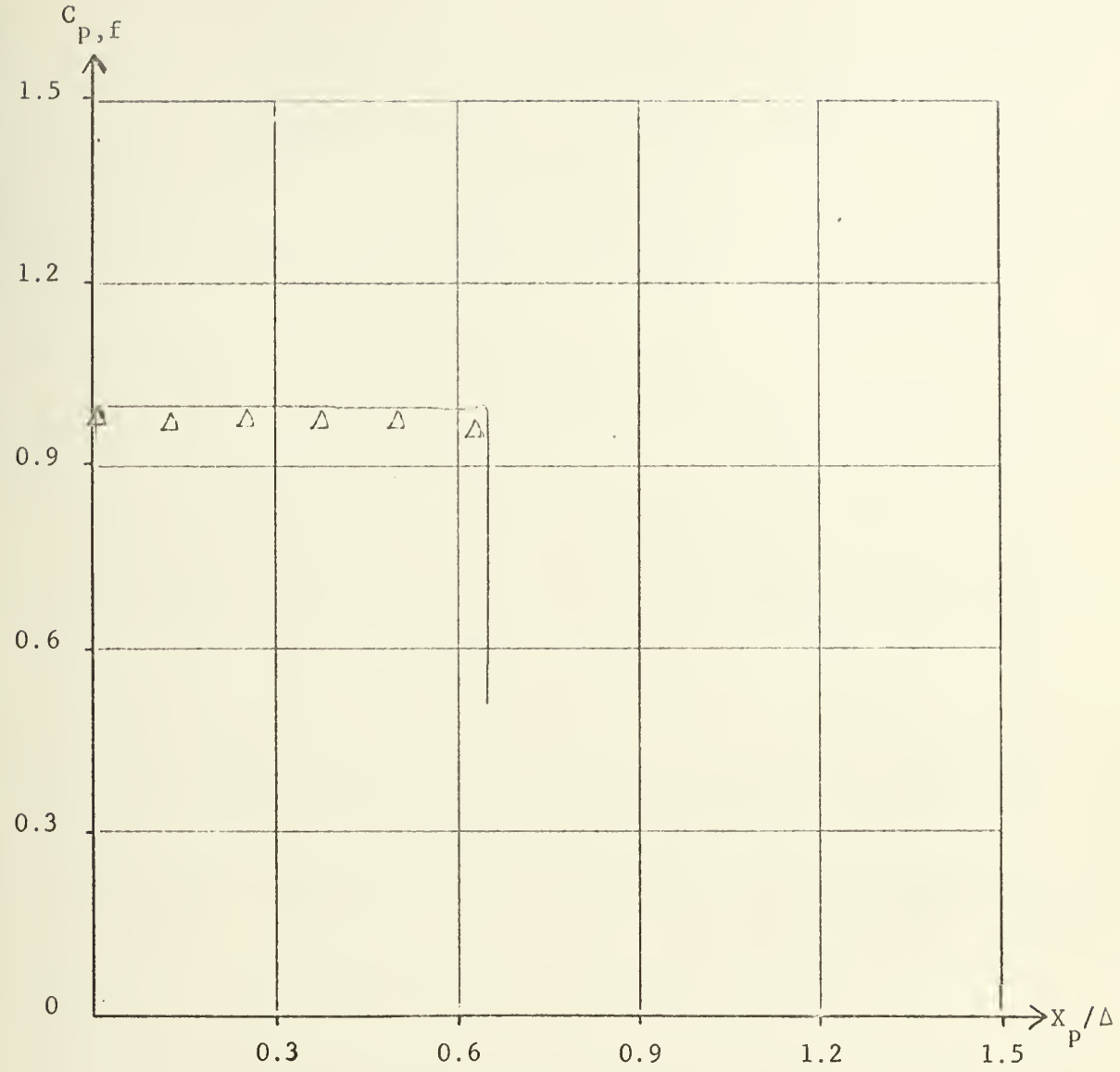

FIGURE 8-3 Pressure coefficient along the fuselage

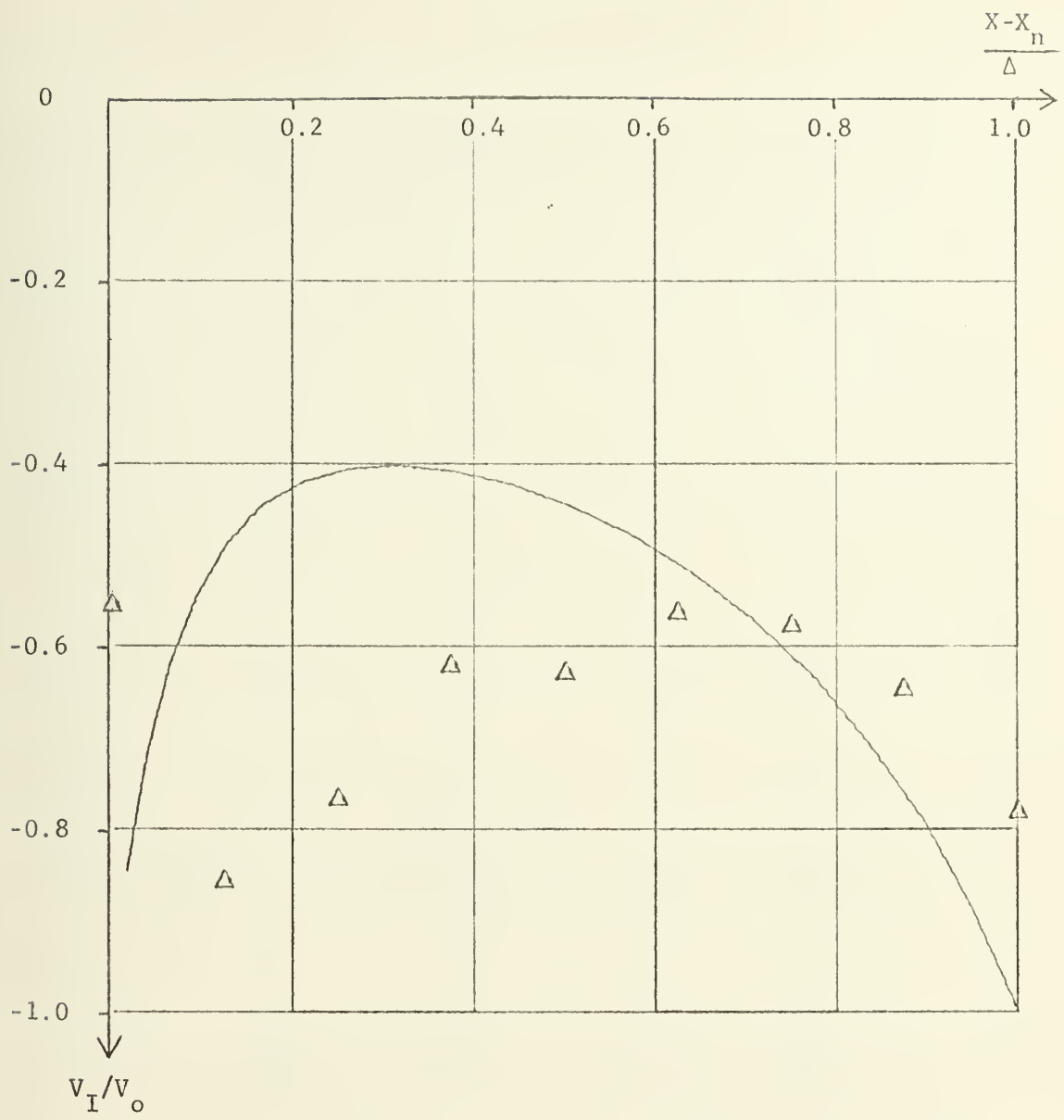

FIGURE 8-4 Velocity profile in the nozzle exit

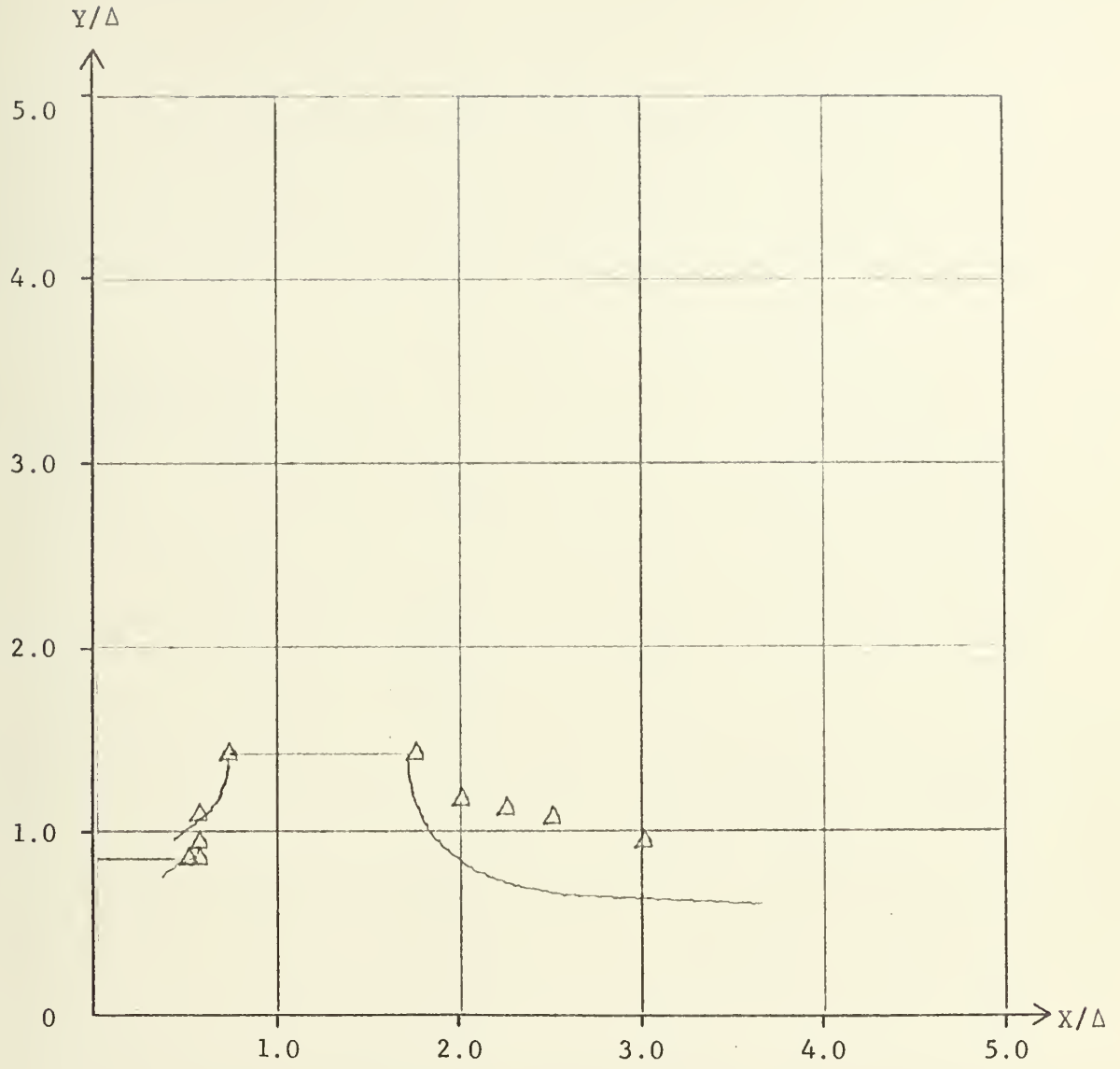

$\frac{X_p}{\Delta} \approx .56$ $\frac{Y_p}{\Delta} \approx .86$ $\frac{X_n}{\Delta} \approx .73$ $\frac{Y_n}{\Delta} \approx 1.43$

$\beta = 90$ $\alpha = 0$

$Re \approx 3900$

FIGURE 9-1 Free streamline plot

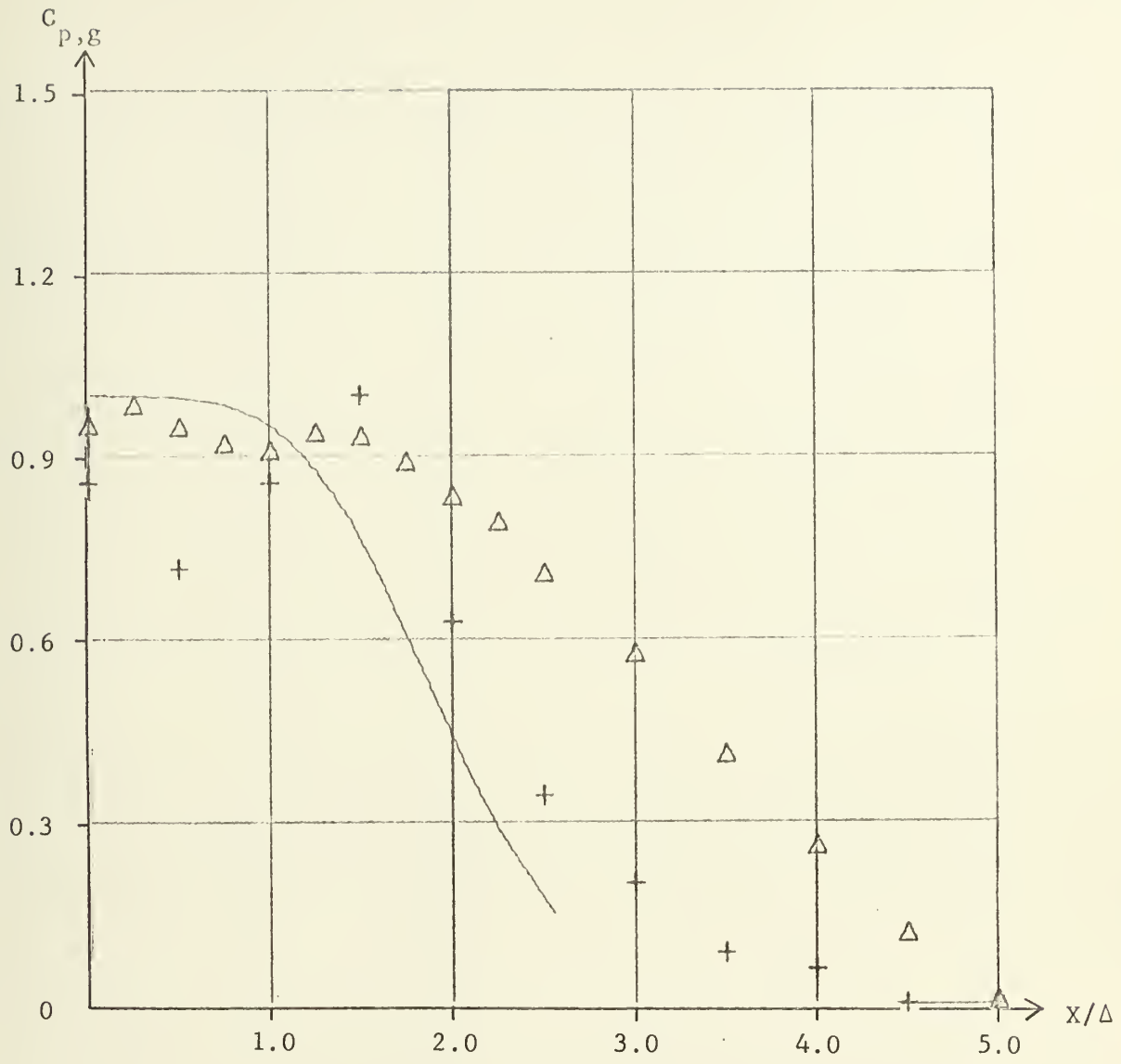

FIGURE 9-2 Pressure coefficient along the ground

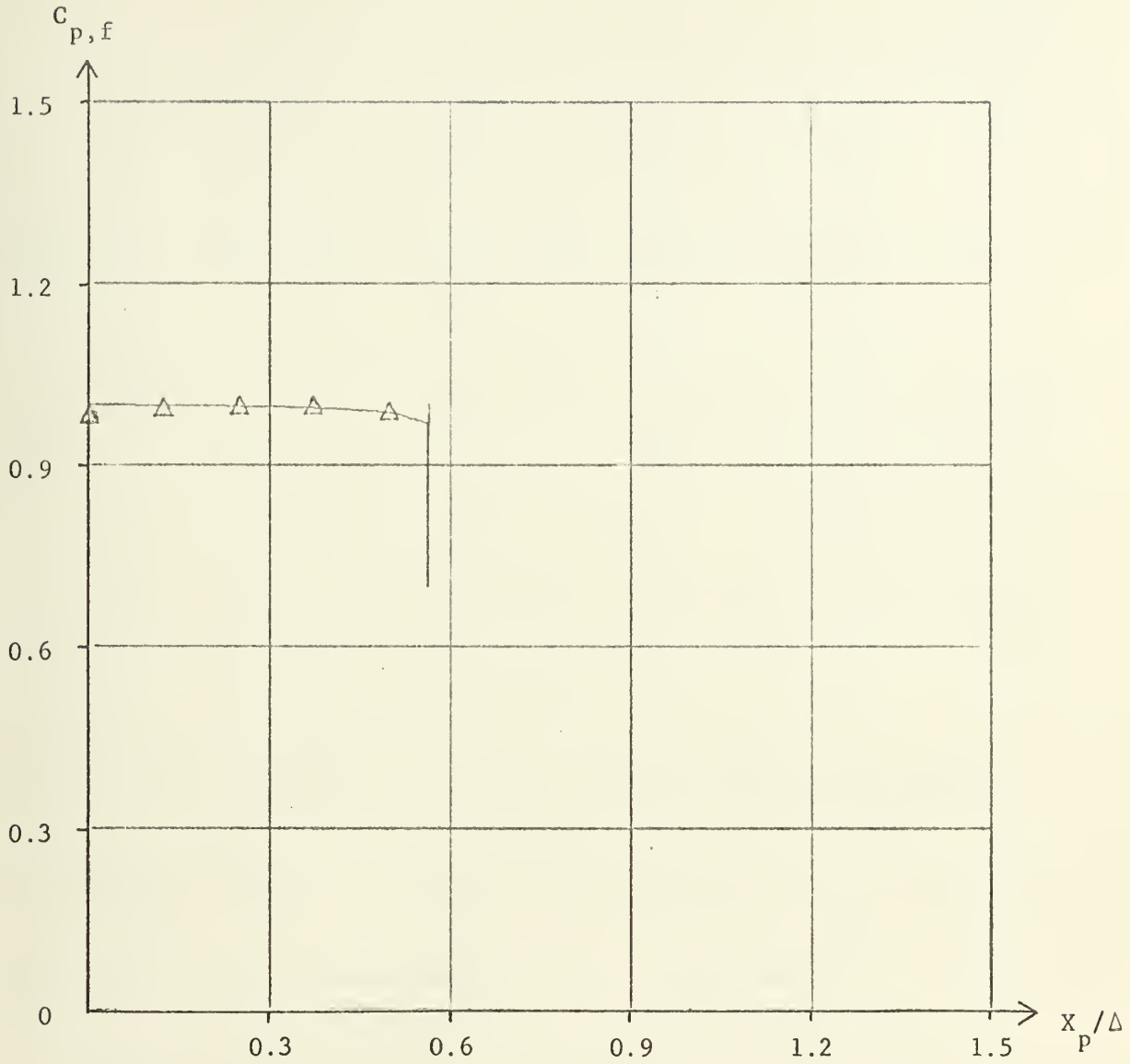

FIGURE 9-3 Pressure coefficient along the fuselage

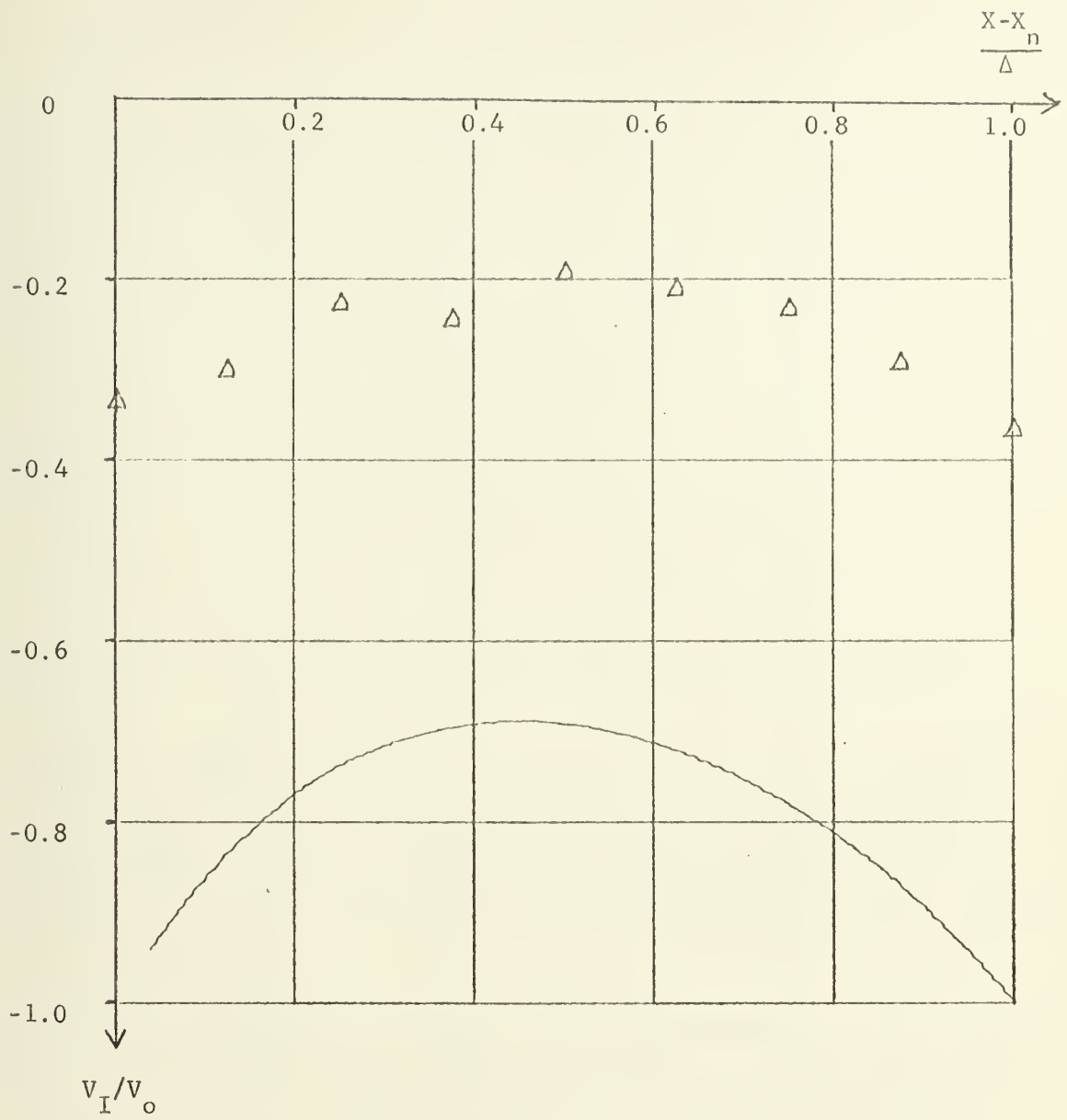

FIGURE 9-4 Velocity profile in the nozzle exit

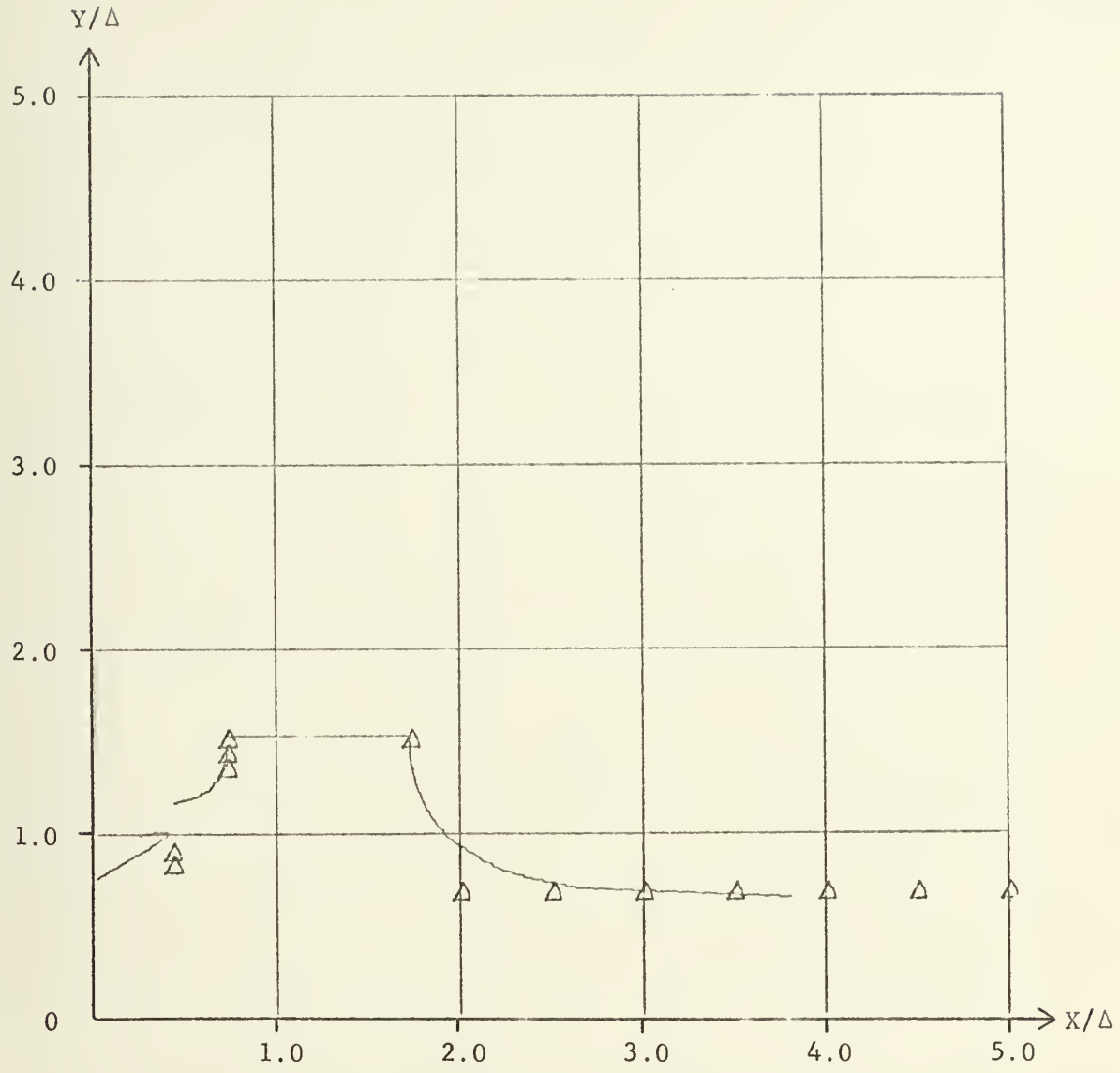

$\frac{X_p}{\Delta} \approx .48$ $\frac{Y_p}{\Delta} \approx .77$ $\frac{X_n}{\Delta} \approx .74$ $\frac{Y_n}{\Delta} \approx 1.53$

$\beta = 60$ $\alpha = 0$

$Re \approx 6800$

FIGURE 10-1 Free streamline plot

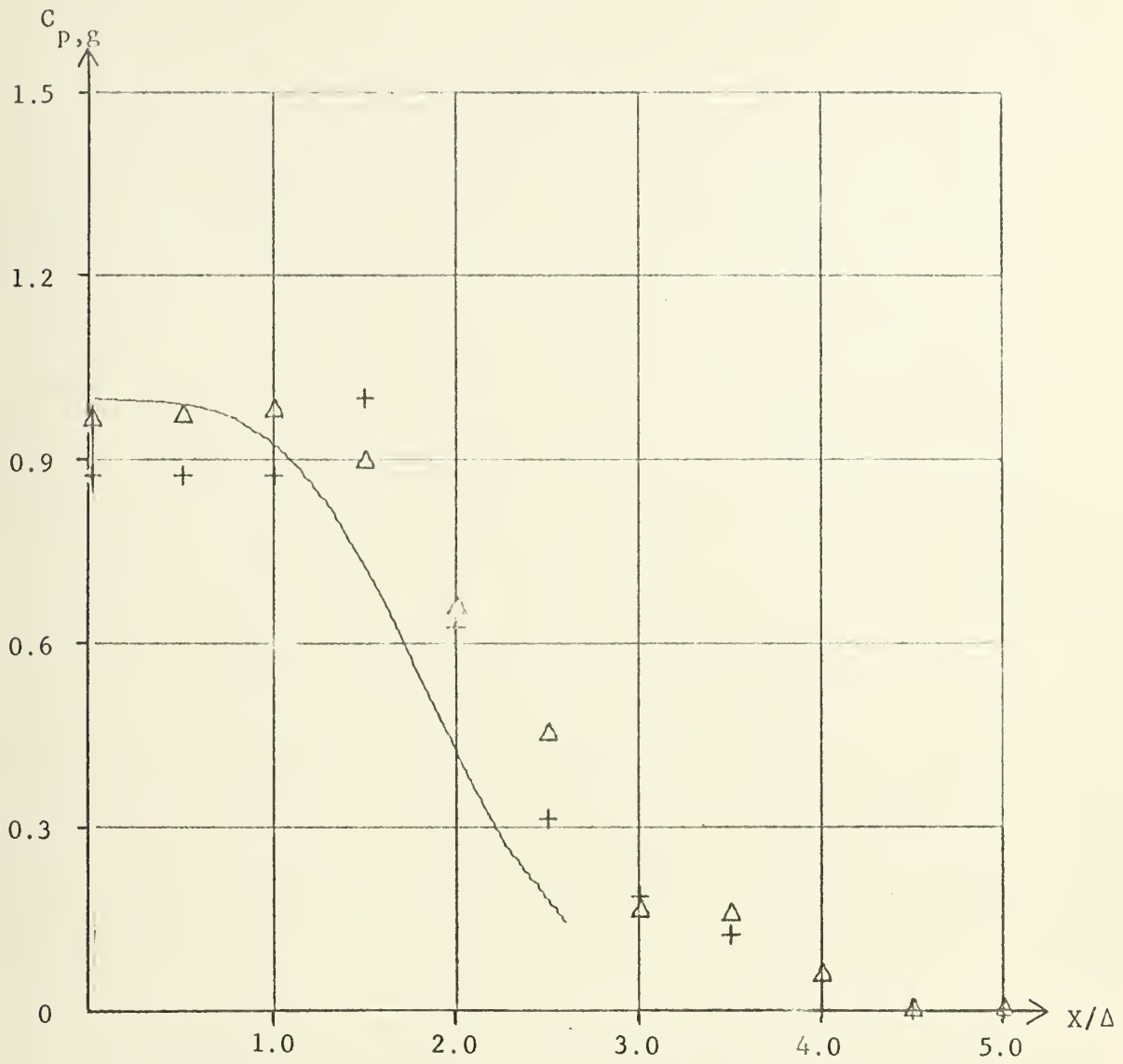

FIGURE 10-2 Pressure coefficient along the ground

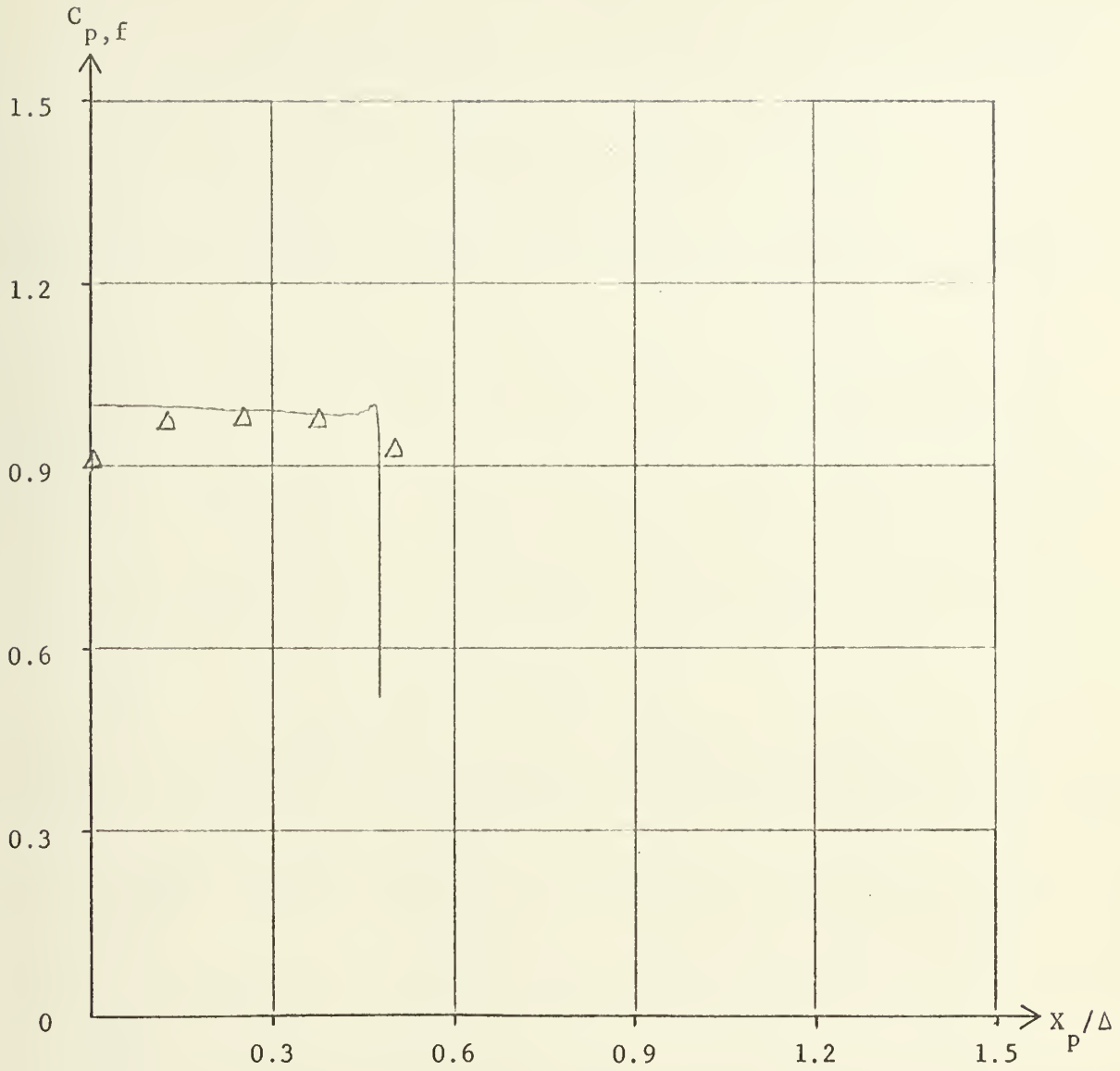

FIGURE 10-3 Pressure coefficient along the fuselage

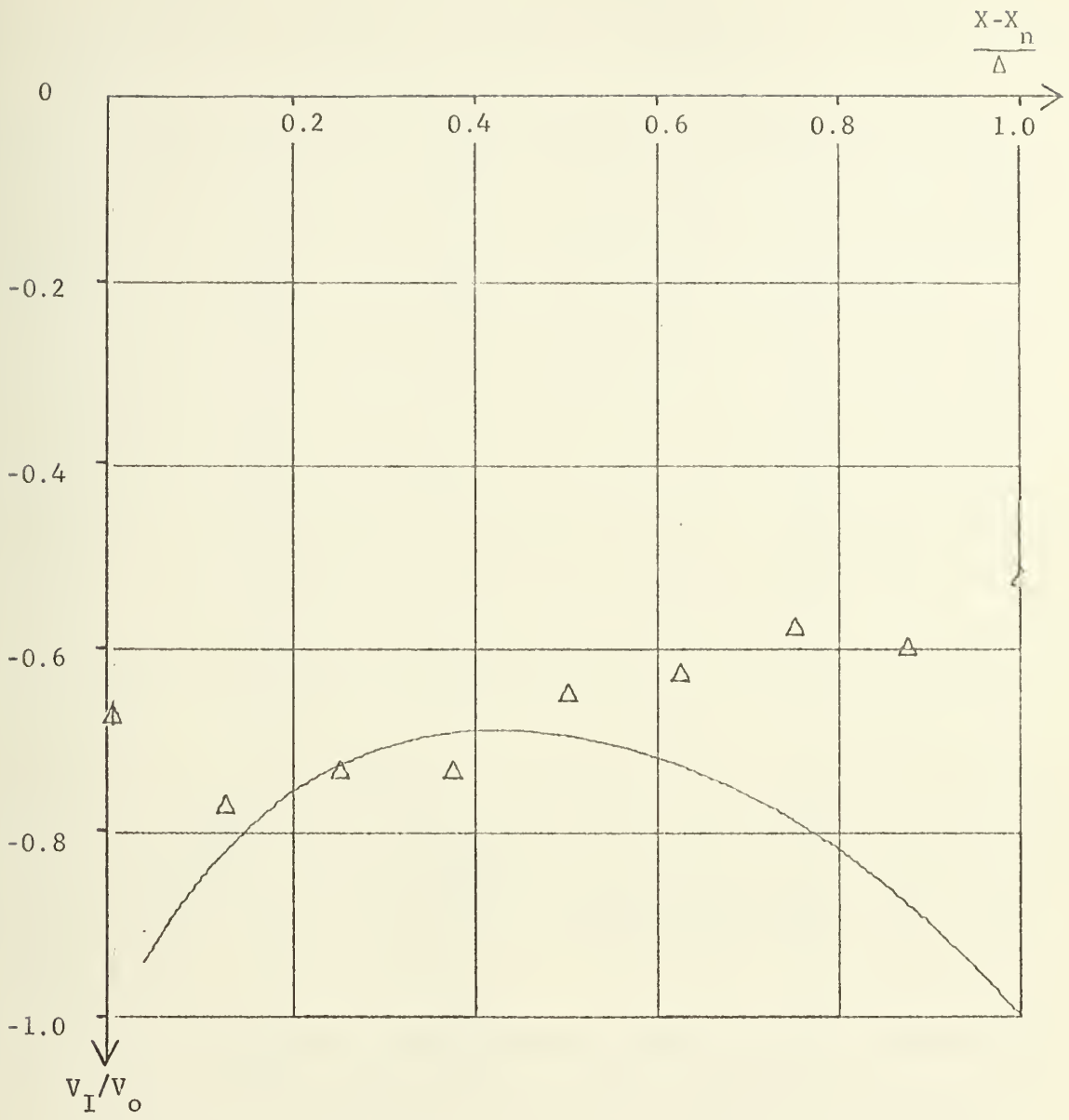

FIGURE 10-4 Velocity profile in the nozzle exit

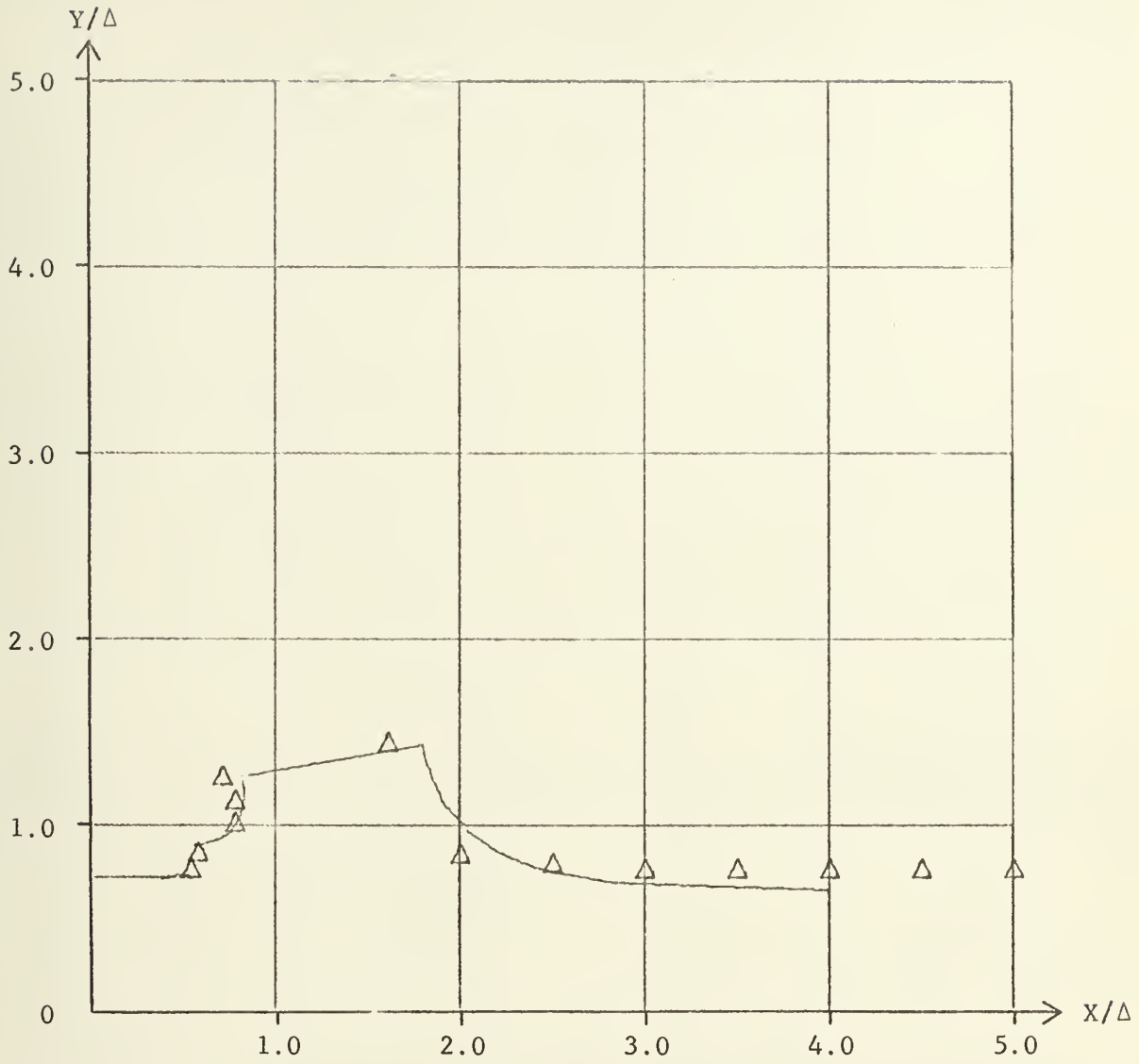

$\frac{X_p}{\Delta} \approx .55$ $\frac{Y_p}{\Delta} \approx .72$ $\frac{X_n}{\Delta} \approx .83$ $\frac{Y_n}{\Delta} \approx 1.26$

$\beta = 90$ $\alpha = 10$

$Re \approx 4200$

FIGURE 11-1 Free streamline plot

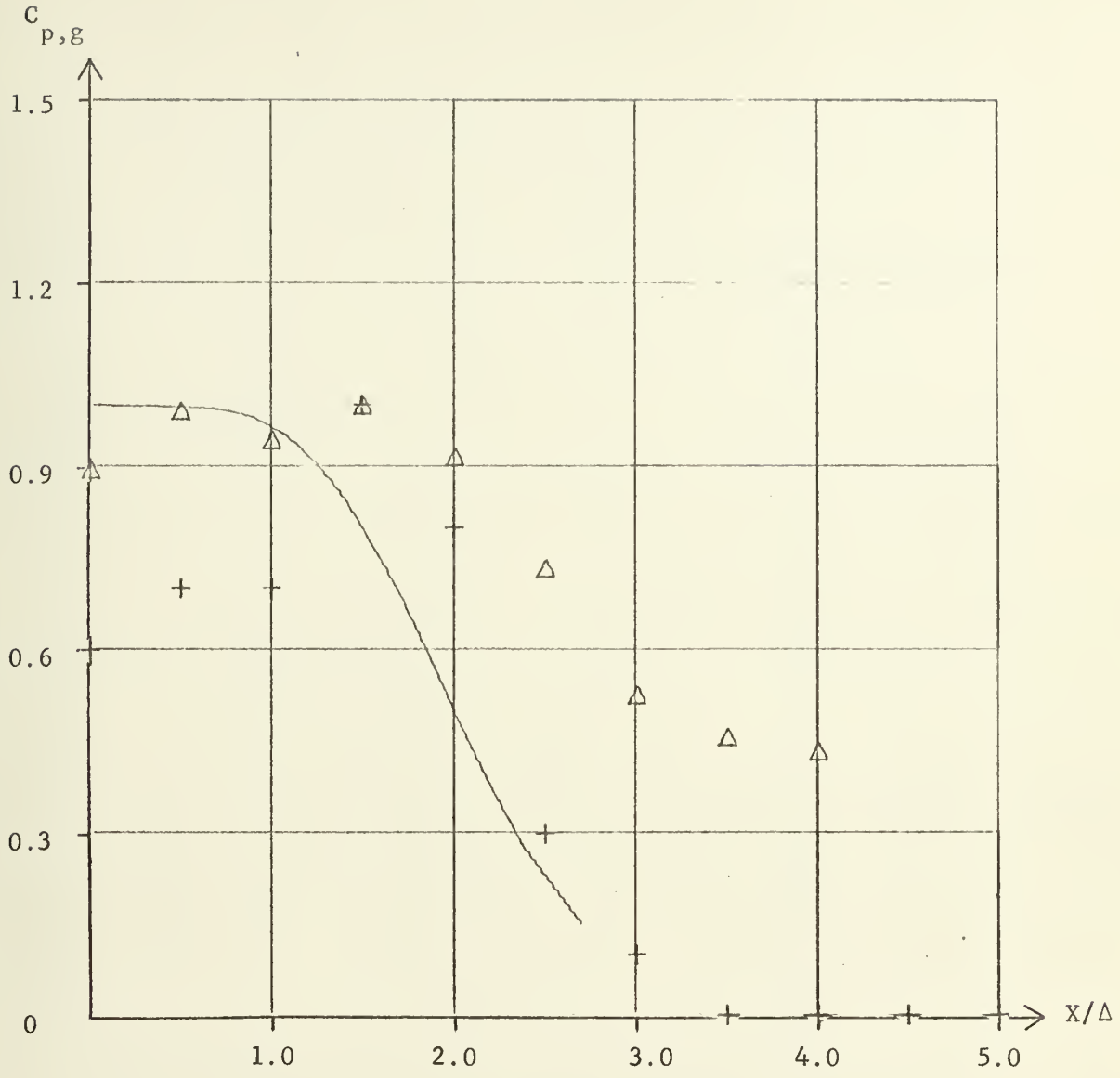

FIGURE 11-2 Pressure coefficient along the ground

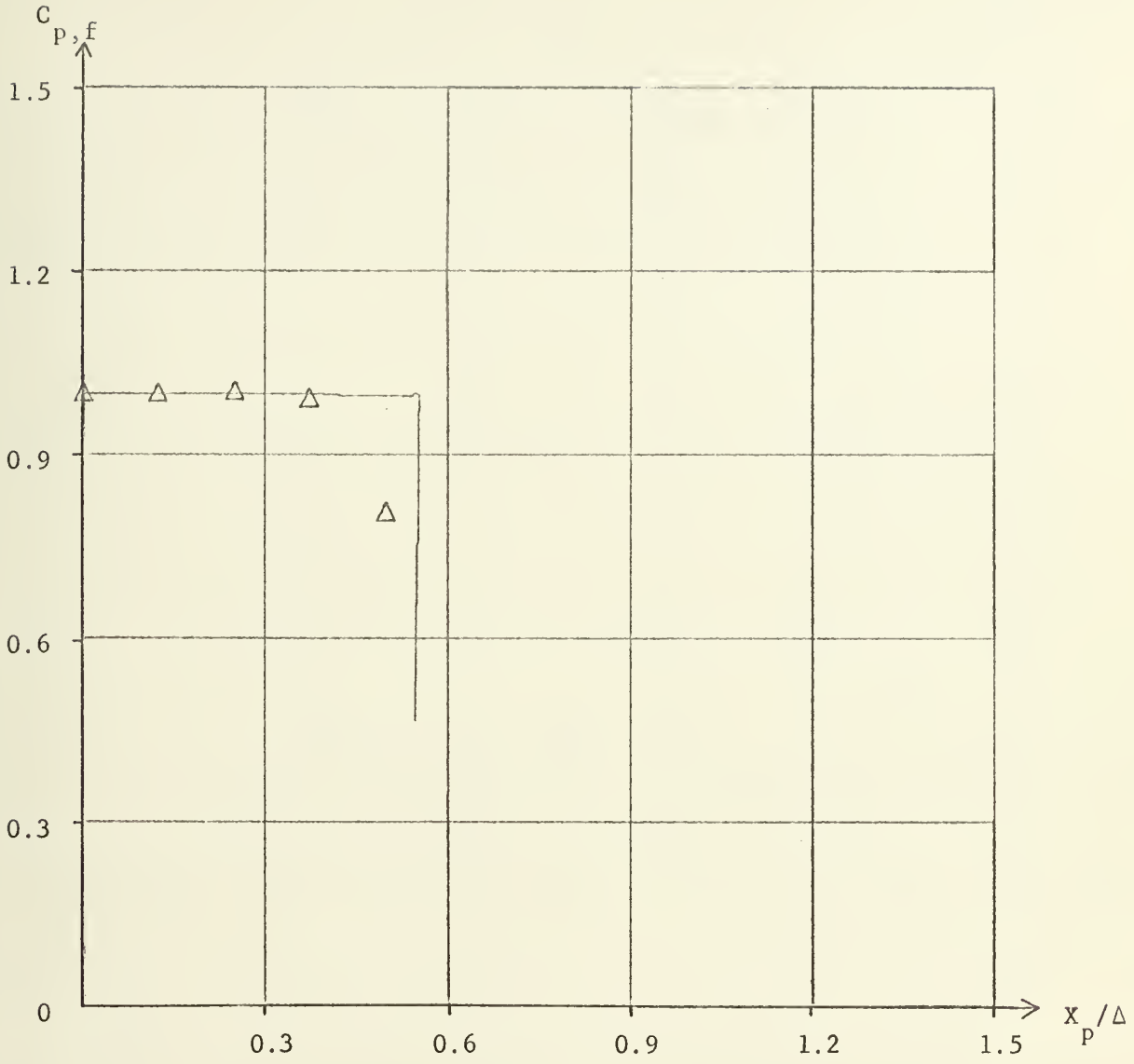

FIGURE 11-3 Pressure coefficient along the fuselage

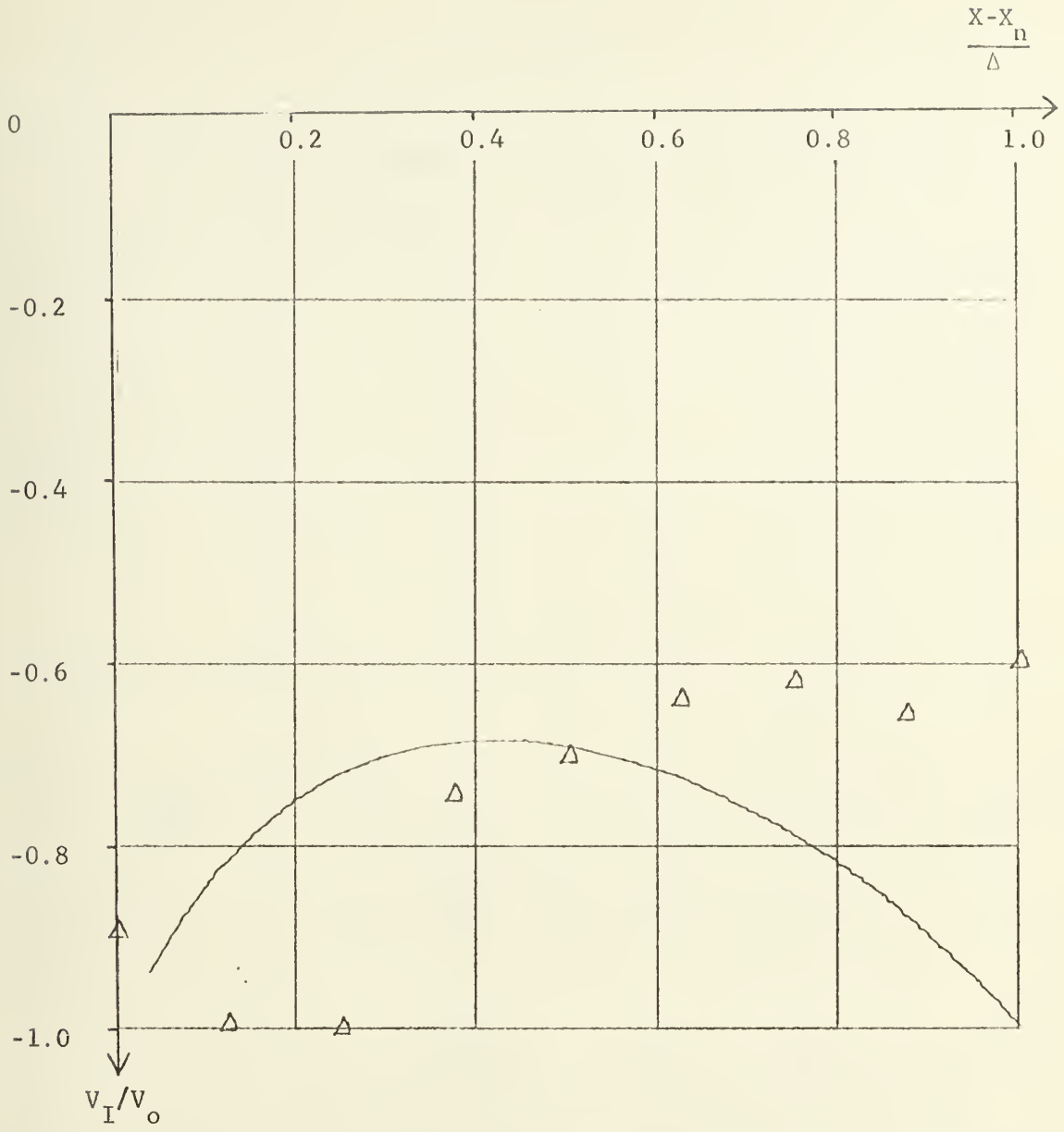

FIGURE 11-4 Velocity profile in the nozzle exit

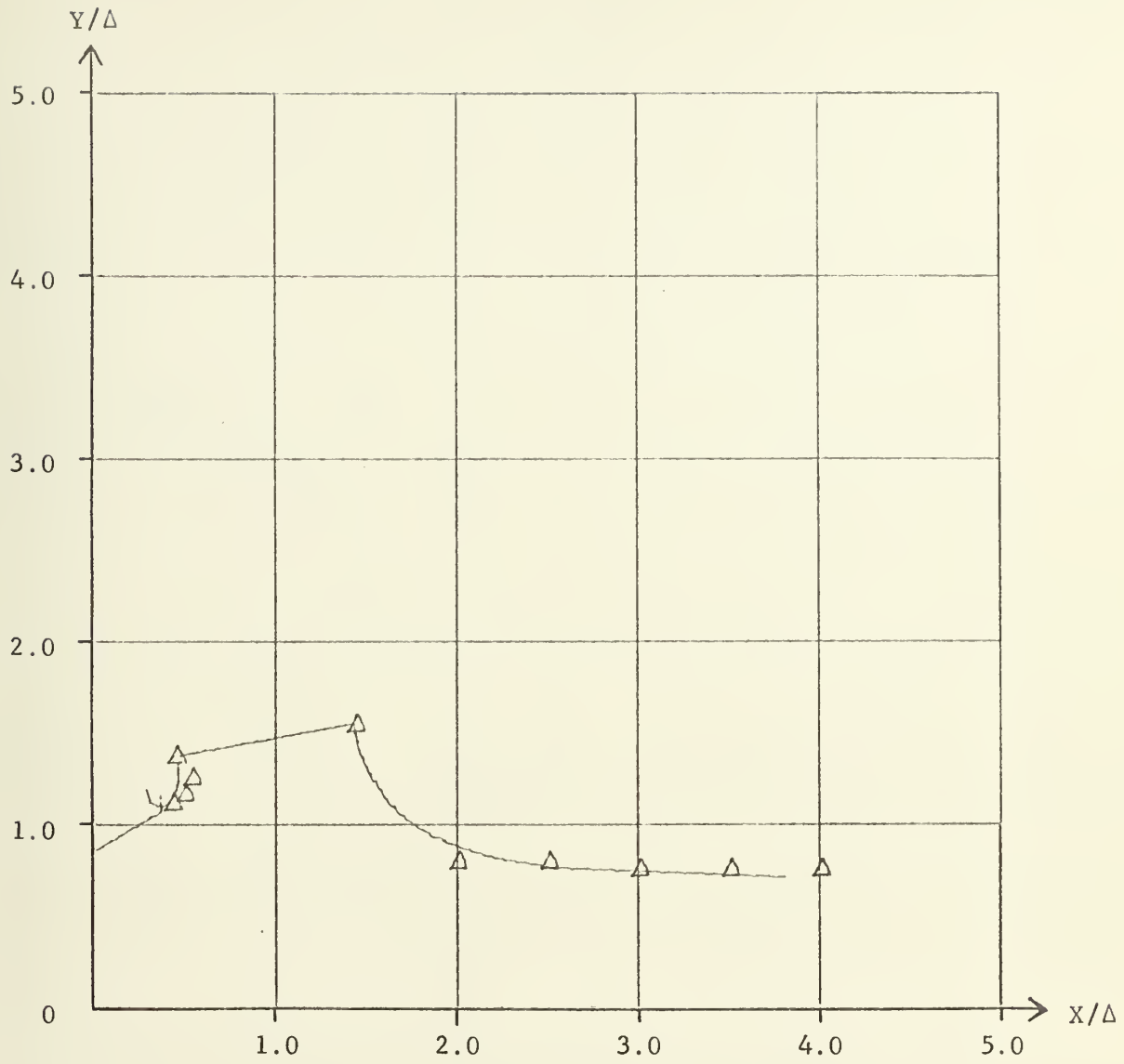

$\frac{X_p}{\Delta} \approx .42$ $\frac{Y_p}{\Delta} \approx .86$ $\frac{X_n}{\Delta} \approx .46$ $\frac{Y_n}{\Delta} \approx 1.38$

$\beta = 60$ $\alpha = 10$

$Re \approx 4700$

FIGURE 12-1 Free streamline plot

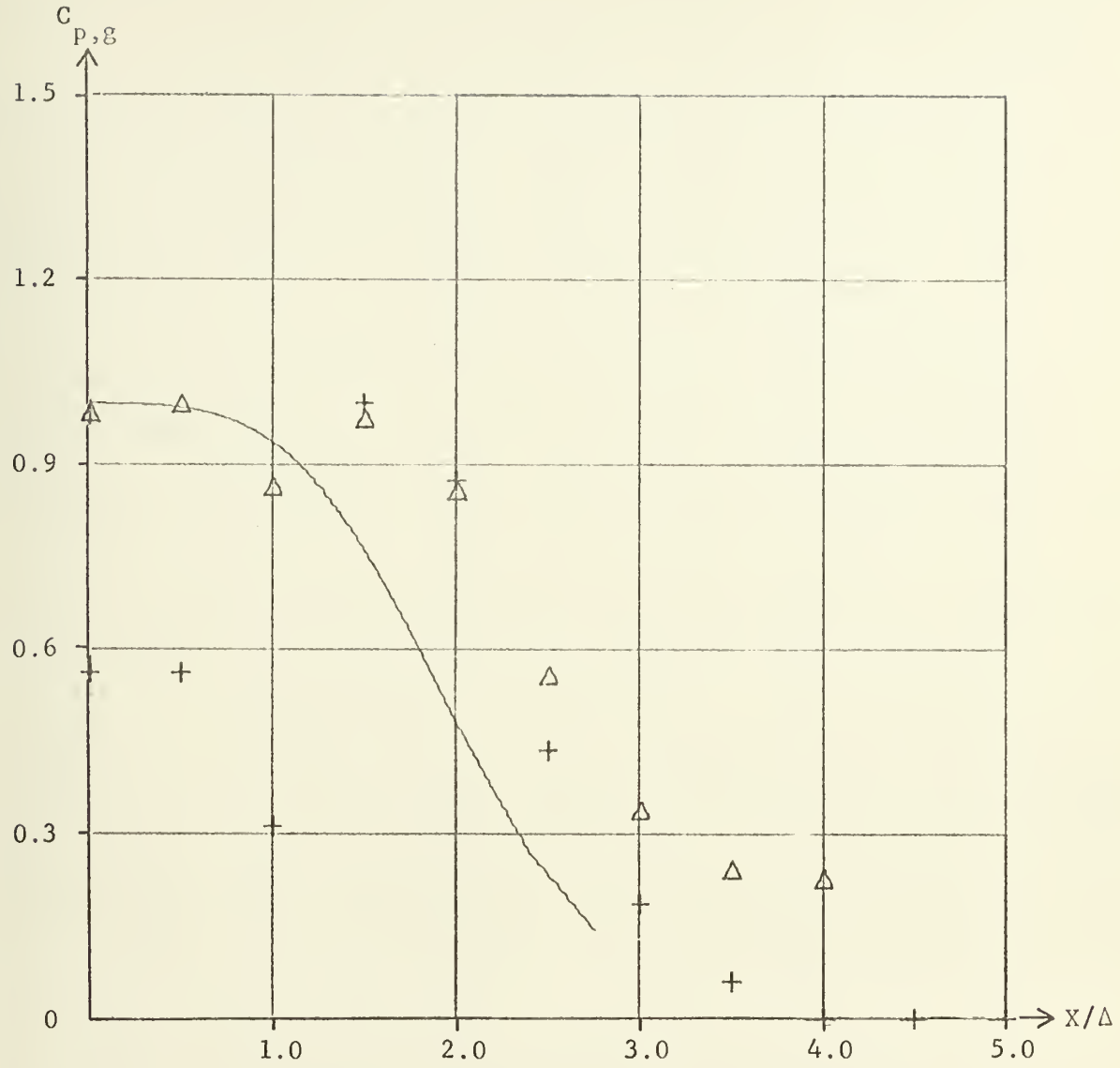

FIGURE 12-2 Pressure coefficient along the ground

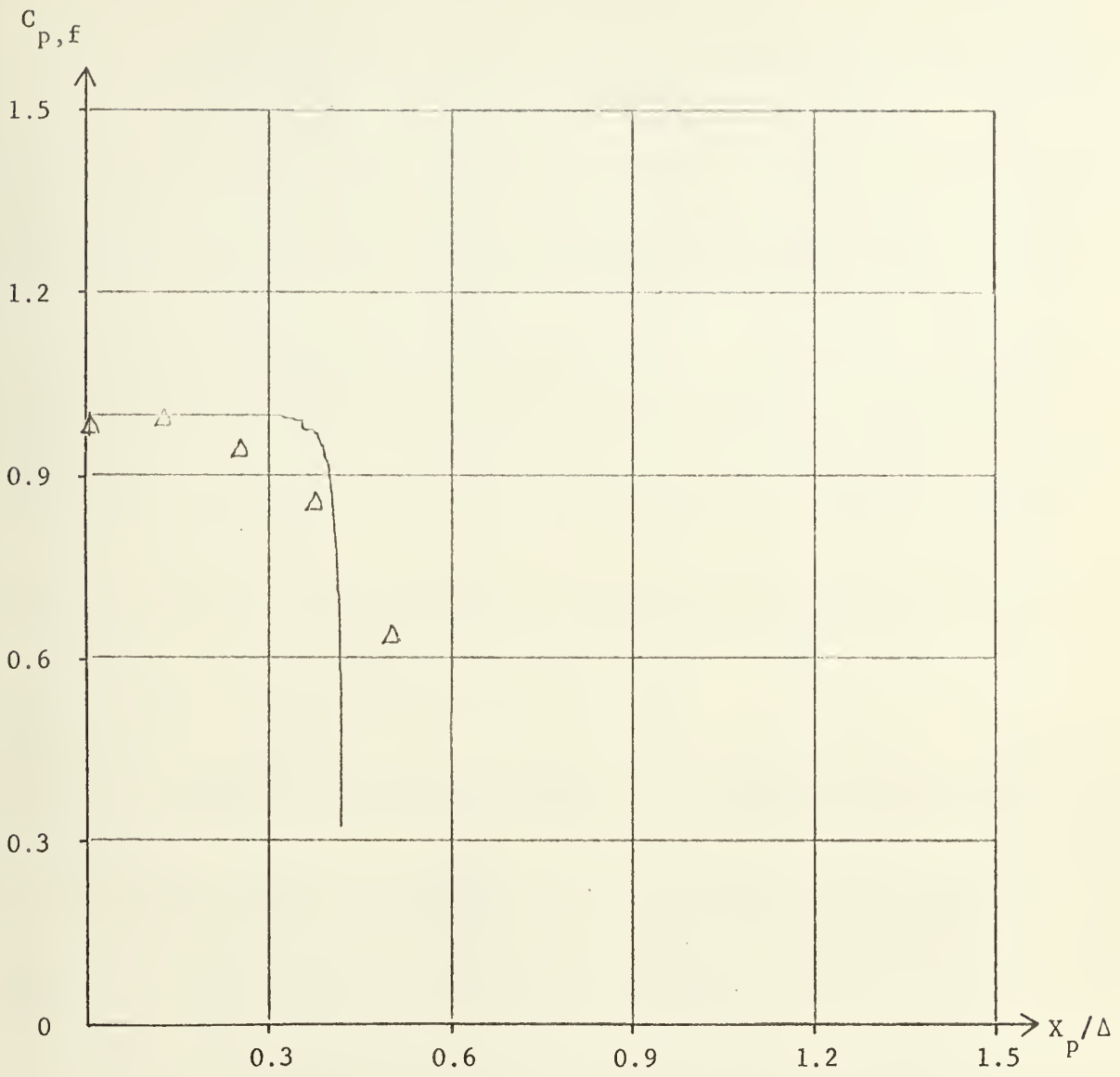

FIGURE 12-3 Pressure coefficient along the fuselage

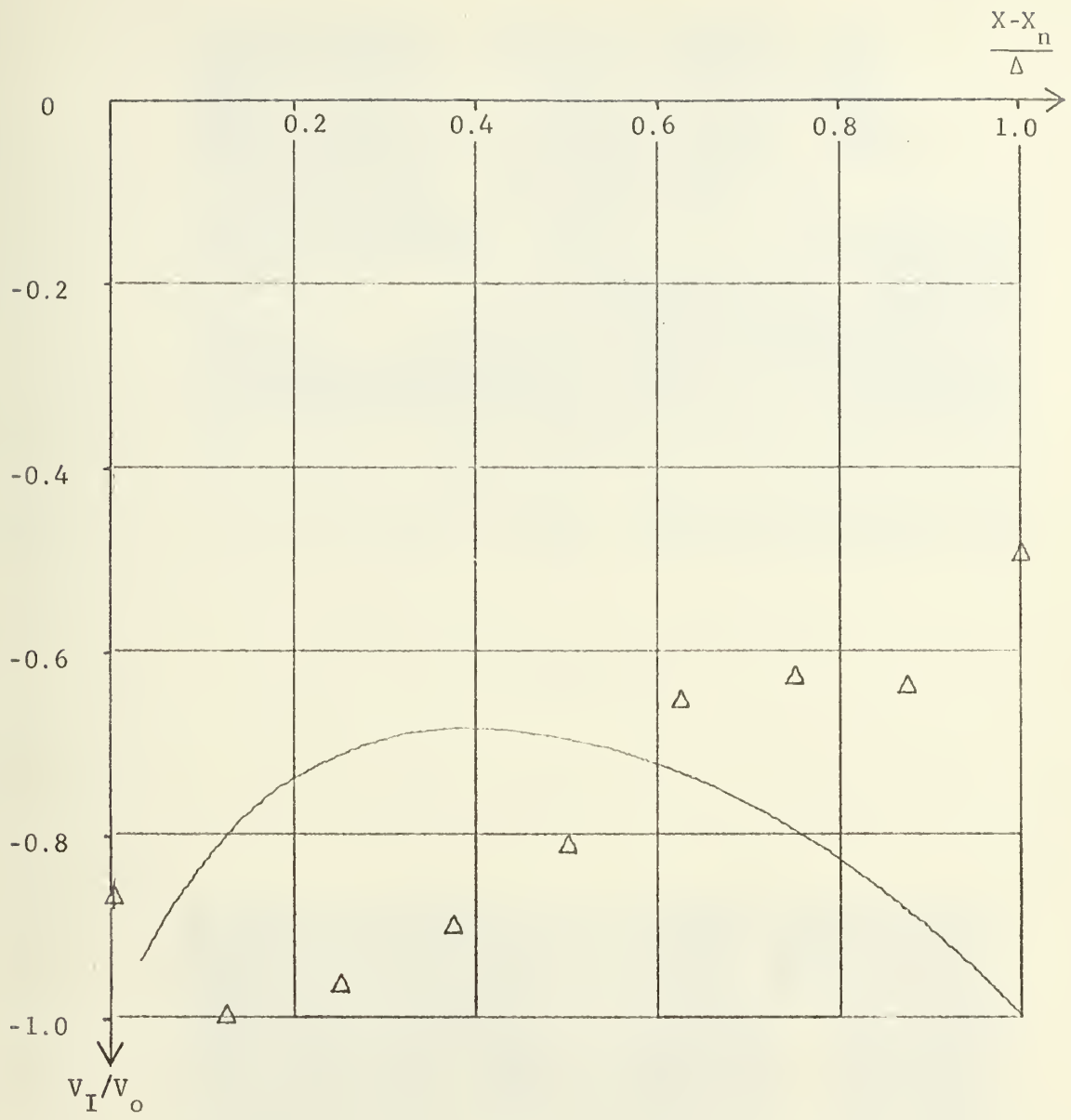

FIGURE 12-4 Velocity profile in the nozzle exit

Tufts of yarn across nozzle exit

FIGURE 13

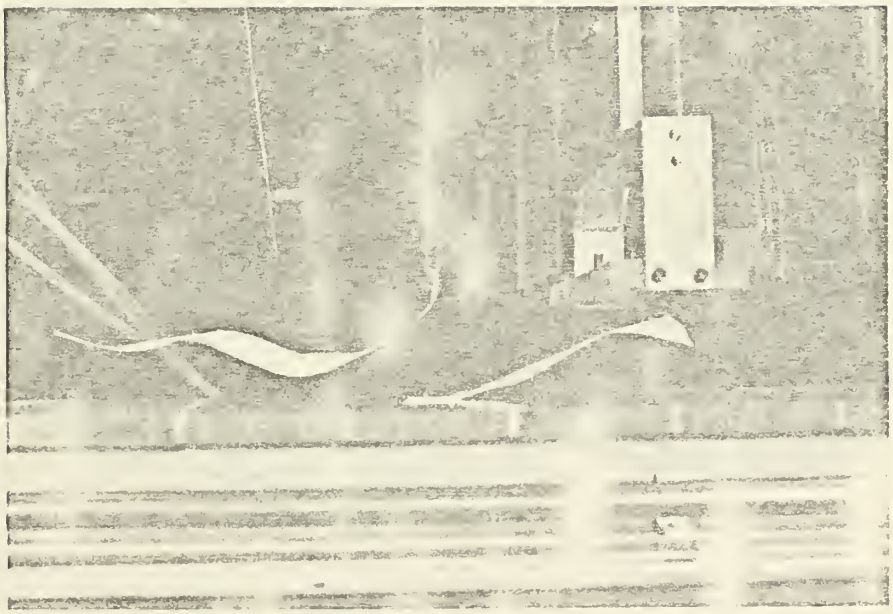

Strips of paper attached to ground plate
and nozzle

FIGURE 14

VIII. DISCUSSION OF RESULTS

Many combinations of the input parameters produced impossible configurations (negative plate heights, etc.). In fact there were far more extraneous solutions than useful ones. There were no combinations found which produced a configuration with the nozzle exit lower than the plate. Very few reasonable configurations resulted from the maximum or minimum values for the parameters.

Most of the configurations of interest were found to have input parameters in the following ranges:

$$.3 \leq k \leq .6$$

$$.1 \leq \delta_L/\delta_R \leq .5$$

$$.6 \leq \eta_F/K' \leq .9$$

$$.1 \leq \xi_A/K \leq .9$$

There were possible configurations outside of these ranges, but most of them had extremely small plate widths. Variation of any one input parameter was not found to change any single physical parameter.

Decreasing the plate angle had a tendency to decrease the plate width and increase the plate height. Tilting the nozzles caused an increase in plate and nozzle height but decreased plate width and nozzle spacing for a given set of abstract input parameters. Neither of these variations had any outstanding effect on the theoretical pressure coefficients.

The experimental data for the streamlines agree quite well with the theoretical plot. The data points between the plate and nozzle often seem to follow a different streamline than the theory. This is a result of the fact that the test plates were of finite thickness, while the

theoretical plates were infinitely thin. Figure 9-1 shows entrainment effects for very high nozzle positions. In some cases the theoretical plot can be very impractical. Notice in Figure 11-1 that the streamline from the edge of the plate turns and passes through the plate.

In most cases the theoretical pressure coefficients along the ground and plate were quite close to the actual situation. The micromanometer data points are somewhat questionable. The pressures were extremely low even for the instrument which was used. The theoretical coefficient is assumed to approach zero after the last point plotted, as the measurements indicate.

The nozzle exit velocity profiles for very low velocities were approximately the same shape as those from the theory, but as the exit velocities become higher the profile becomes much flatter. In all cases it should be remembered that the velocity data points are normalized with the maximum velocity for that particular test. In most cases this maximum velocity was found to be near the ground two or three nozzle widths from the high pressure region beneath the fuselage and nozzle exit. Hence, the data points tend to be displaced from the theoretical profile which assumes that the maximum velocity is reached at the edges of the nozzle exit. In all cases the profile was somewhat affected by the presence of the wall of the nozzle.

The motion of the tufts of yarn placed in the nozzle exit (Figure 13) show the manner in which the flow divides to the left and right of the nozzle. The strips of paper attached to the nozzle exit and ground plate in Figure 14 show the stream of flow away from the nozzle an the upward air currents under the fuselage.

IX. CONCLUSIONS

The experiments have not only verified the theory, but have also pointed out its limitations. The analytical results were quite accurate for nozzles very close to the plate and the ground. As the nozzles were moved higher the effects of entrainment became more noticeable. The pressure distribution along the ground was not as uniform as that predicted by the analysis.

The greatest limitation on the theory, however, is not the restricted nozzle positions, but the fact that the analytical solution depends upon four parameters in an abstract plane. Since there is no direct connection between any one of these parameters and the physical parameters of plate height and width and nozzle height and spacing, the theoretical results are only possible after an iteration process to find the proper input parameters. A vast amount of computer time is required to solve for relatively few configurations.

X. RECOMMENDATIONS

The theoretical solution could possibly be extended to include other fuselage shapes. However, perhaps a more practical approach would be to develop analytical solutions in terms of physical parameters. A solution of this type would be a useful tool to the aircraft designer.

Further tests should be carried out with higher nozzle exit velocities to determine the effects of extremely turbulent flow underneath the aircraft. Also of interest would be the effect of crosswinds on the flow and the pressure distribution.

Reference 1 mentions the use of a special takeoff grating to virtually eliminate entrainment effects on aircraft using a single central jet exhaust. No information was available concerning the effects of such a grating on multi-jet configurations. Tests of a takeoff grating mounted on the existing apparatus would be of interest to determine the resulting changes in ground effect.

There were no reasons given for restricting δ_L/δ_R to values less than one. Obviously there must be solutions for nozzle exits lower than the plate height. If the equations can be satisfied by values of δ_L/δ_R greater than one, perhaps this will lead to the lower nozzle positions.

APPENDIX A

To obtain analytical solutions for the flow field beneath a V/STOL aircraft Siegel and Goldstein [Ref. 3] considered a simplified two-dimensional model of the flow. The following is a condensation of their analysis.

The aircraft under consideration has a fan pod or jet exhaust in each wing. As the two jets strike the ground they divide into flows to the left and right. The colliding flows beneath the aircraft rise and strike the fuselage. The bottom of the fuselage is represented by a flat plate which can be at an angle with the ground. Because of symmetry only half of the flow field is considered.

The flow is assumed to be incompressible, inviscid, irrotational, isothermal and steady. The velocity at the nozzle exit is taken to be perpendicular to the exit plane. The surrounding fluid is at rest and entrainment is ignored. If the nozzle exits are within a few jet widths of each other and of the ground, the inviscid solution with no entrainment is a reasonable approximation of the actual flow conditions. With these restrictions the flow has been reduced to a free streamline problem with constant pressure surroundings.

Figure A1-1 shows the physical boundaries of the flow field. Defining the complex conjugate velocity as

$$\zeta = u - iv \tag{A1}$$

and the complex potential as

$$W = \Phi + i\psi \tag{A2}$$

the flow regions in the hodograph and complex potential planes are shown in Figures A1-2 and A1-3.

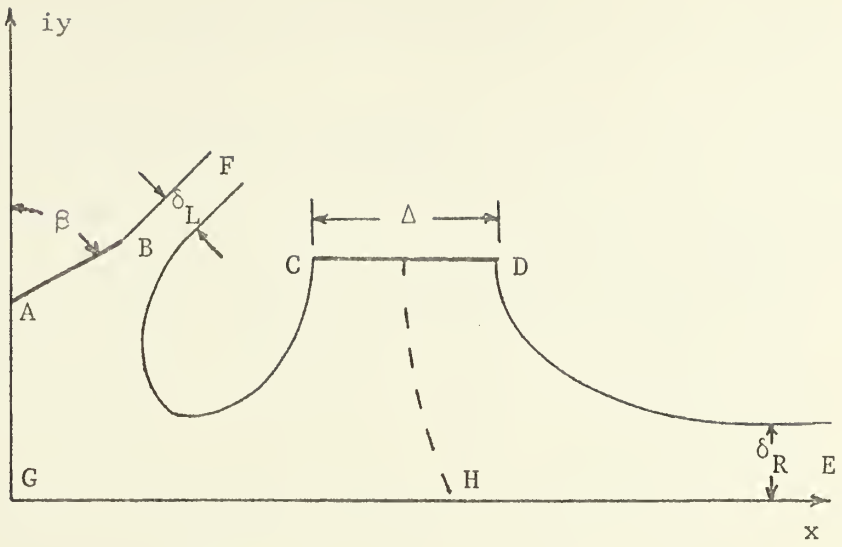

FIGURE A1-1 Physical flow field

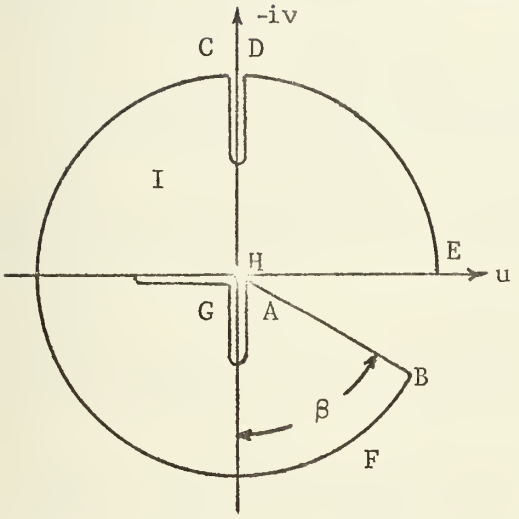

FIGURE A1-2 Hodograph plane

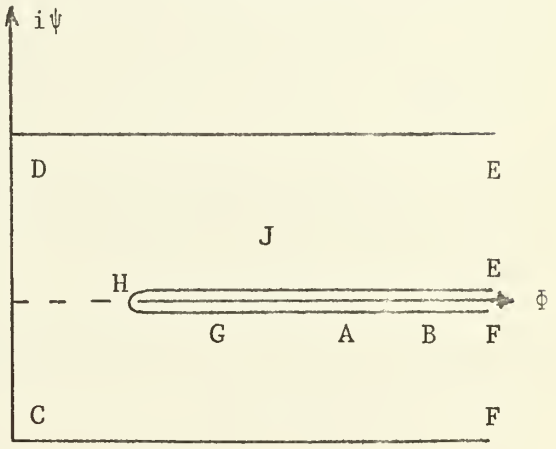

FIGURE A1-3 Complex potential plane

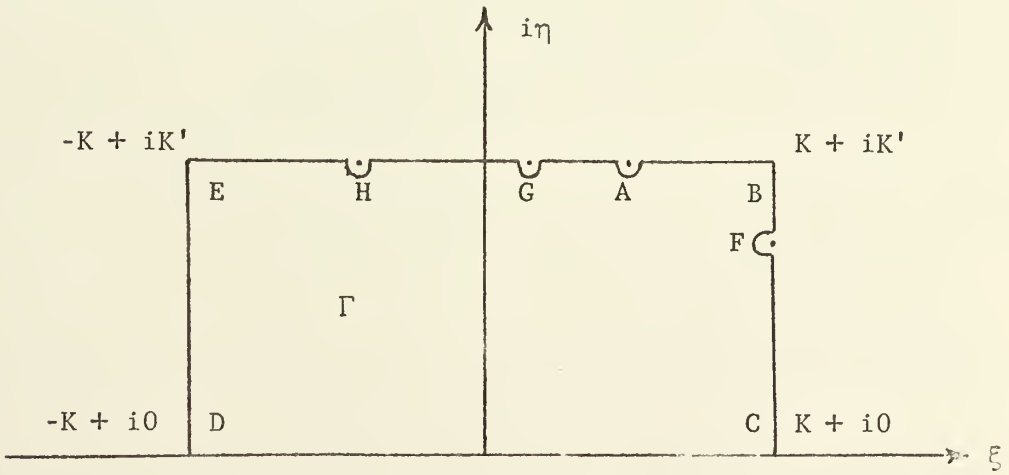

FIGURE A1-4 T-plane

The solution in the physical plane is obtained by performing the integration

$$z = \int \frac{1}{\zeta} \, dW + \text{constant} \tag{A3}$$

In order to perform this integration ζ and W must be expressed in terms of the same variables. This is accomplished by mapping the rectangular region Γ of the T-plane onto the ζ and W planes.

The function which maps the region Γ onto the hodograph plane is

$$\zeta(T) = V_o e^{i(\pi/2)} \Omega(T;\xi_H,k) \sqrt{\Omega(T;\xi_G,k)} \, [\Omega(T;\xi_A,k)]^{\beta/\pi} \tag{A4}$$

The Omega functions are defined in Ref. 4 to be

$$\Omega(T;\xi_r,k) \equiv \frac{\theta_4\left(\frac{\pi}{4K}(T-\xi_r)\middle|\frac{iK'}{2K}\right)}{\theta_4\left(\frac{\pi}{4K}(T+\xi_r-2K)\middle|\frac{iK'}{2K}\right)} \tag{A5}$$

where θ_4 is the fourth theta function which is defined in Ref. 8 as follows:

$$\theta_4(z|\tau) = 1 + 2 \sum_{n=1}^{\infty} (-1)^n e^{i\pi n^2 \tau} \cos 2nz \tag{A6}$$

The relationship between ξ_A, ξ_G and ξ_H must satisfy the requirement that on the plate the argument of $\zeta(T)$ must equal the direction along the plate. By using the formulas for the arguments of the Omega functions presented in Ref. 4 it can be shown that

$$\left(\frac{\pi}{4} + \frac{\beta}{2}\right)\frac{4K}{\pi} = 2\xi_H + \xi_G + \frac{2\beta}{\pi}\xi_A \tag{A7}$$

By applying a Schwarz-Christoffel transformation the upper half of an intermediate t-plane (not illustrated) is mapped onto the complex potential plane. A second transformation maps the T-plane onto the upper half of the t-plane. By eliminating t between these two transformations, the function which maps the T-plane onto the W-plane is found to be

$$\frac{dW}{dT} = iA \frac{(k \text{ sn } \xi_H \text{ sn } T - 1) \text{ dn } T}{(1 + k \text{ sn } T)\ [1\text{-dn}(\eta_F, k') \text{ sn } T]} \tag{A8}$$

where A is a constant.

Using partial fractions, integrating equation (A8) and applying the condition that the flow through the nozzle exit is equal to the difference in the stream function across the exit, the value of A can be found in terms of the average nozzle exit velocity.

Noting that the flow to the left beneath the nozzle is equal to the change in the imaginary part of the complex potential at F and requiring the velocity at that point to be the free streamline velocity we have

$$\delta_L V_o = \bar{V}_I \Delta \frac{k + \text{dn } (\eta_F, k') - k\ (1 + \text{sn } \xi_H)}{k + \text{dn } (\eta_F, k') - k\ (1 + \text{sn } \xi_H)\ [1 - \text{sn } (\eta_F, k')]} \tag{A9}$$

Since continuity requires that

$$\delta_R V_o + \delta_L V_o = \Delta \bar{V}_I \tag{A10}$$

we can eliminate δ_L from equation (A9) and have

$$\frac{\delta_R}{\Delta} = \frac{\bar{V}_I}{V_o} \frac{k\ (1 + \text{sn } \xi_H) \text{ sn } (\eta_F, k')}{k + \text{dn } (\eta_F, k') - k\ (1 + \text{sn } \xi_H)\ [1 - \text{sn } (\eta_F, k')]} \tag{A11}$$

By dividing equation (A11) by equation (A9) and rearranging

$$\text{sn } \xi_H = \frac{\delta_R/\delta_L \text{ dn } (\eta_F, k') - k \text{ sn } (\eta_F, k')}{\delta_R/\delta_L \ k + k \text{ sn } (\eta_F, k')} \tag{A12}$$

Since ζ and W are both known in the T-plane the solution of equation (A3) becomes

$$z = \int_{\xi_G + iK'}^{T} \frac{1}{\zeta(T)} \frac{dW}{dT} \, dT \tag{A13}$$

or after substitution

$$\frac{z}{\Delta} = \left(\frac{\bar{V}_I}{V_o}\right) \frac{k'}{\pi} \left[\frac{sn\ (\eta_F, k') + \delta_R/\delta_L}{1 + \delta_R/\delta_L}\right]$$

$$X \int_{\xi_G + iK'}^{T} \frac{(k\ sn\ \xi_H\ sn\ T - 1)\ (1 - k\ sn\ T)\ dT}{dn\ T\ [1 - dn(\eta_F, k')\ snT]\ \Omega(T;\xi_H,k)\sqrt{\Omega(T;\xi_G,k)}\ [\Omega(T;\xi_A,k)]^{\beta/\pi}} \tag{A14}$$

Using this relation the ratio of the average velocity in the nozzle exit to the free stream velocity is

$$\frac{\bar{V}_I}{V_o} = M \left[\frac{1 + \delta_R/\delta_L}{sn\ (\eta_F, k') + \delta_R/\delta_L}\right] \tag{A15}$$

where

$$M \equiv \left\{\frac{k'}{\pi} \int_{-K}^{K} \frac{(1 - k\ sn\ \xi_H\ sn\xi)\ (1 - k\ sn\xi)\ d\xi}{dn\xi\,[1 - dn(\eta_F, k')sn\xi]\,\Omega(\xi;\xi_H,k)\sqrt{\Omega(\xi;\xi_G,k)}\,[\Omega(\xi;\xi_A,k)]^{\beta/\pi}}\right. \tag{A16}$$

The pressure coefficient at a point (x_1, y_1) is

$$C_p = \frac{P(x_1, y_1) - P_o}{1/2\ \rho\ V_o^2} \tag{A17}$$

Using Bernoulli's equation the pressure coefficients on the ground and on the fuselage are

$$C_{p,g} = 1 - \left[\frac{u\ (\xi, K')}{V_o}\right]^2 \qquad -K \leq \xi < \xi_G$$

and (A18)

$$C_{p,f} = 1 - \left[\frac{u^2\ (\xi, K') + v^2\ (\xi, K')}{V_o^2}\right] \qquad \xi_A \leq \xi \leq K$$

The flow field is governed by five physical parameters: plate height, plate width, plate angle, nozzle height and nozzle spacing. Only the plate angle β appears in the solution. Hence the other parameters must

be found in terms of four parameters in the T-plane. Siegel and Goldstein used k, δ_L/δ_R, η_F/K' and ξ_A/K as input parameters for a computer program to plot numerical results. All four parameters have values between zero and one but no representative values and their corresponding physical configurations were available.

```
REF:   NASA TND 5C64
AND NASA TND 5288
CATA SET MUST BE ARRANGED IN THE FOLLOWING ORDER:
TITLE OF FLOW FIELD PLOT
TITLE OF GROUND PRESSURE COEFFICIENT PLOT
TITLE OF PLATE PRESSURE COEFFICIENT PLOT
TITLE OF VELOCITY PROFILE PLOT
VALUE OF BETA,,,ALPHA  IN RADIANS
EMOD,,,DLDR,,,ETAK,,,XIK
NUMBER OF DATA POINTS FOR STREAMLINES,,,FOR GROUND,,,FOR PLATE   FOR NOZZLE
MAXIMUM VOLTAGE RECORDED,,,ZERO VELOCITY VOLTAGE,,,SLOPE OF CALIBRATION CURVE
X,,,Y COORDINATES OF STREAMLINES
X COORDINATES,,,VOLTAGE FOR GROUND
X COORDINATES,,,PRESSURE ON GROUND IN INCHES OF WATER
X COORDINATES,,,VOLTAGE FOR PLATE
X COORDINATES ,,,VOLTAGE FOR NOZZLE EXIT
ALL INTEGRATION SUBROUTINES USE GAUSS 9-POINT QUADRATURE FORMULA
ETA AND XI ARE COORDINATES OF T-PLANE
ITITLE,KTITLE, LTITLE, MTITLE AND LABEL ARE FOR INPUT TO SUBROUTINE DRAW
      EXTERNAL R4,R1,FCT,BIGM,BIGXP,BIGYP,AC',T3,T4,BFX,BFY,YE,DE,EX
    1 FORMAT(F10.5)
    2 FORMAT('  BETA IS ',F10.5,'   ALPHA IS  ', F10 5)
    3 FORMAT(8F10.4)
    7 FORMAT(4F10.5)
    8 FORMAT(' ',2X,'EMOD',5X,'DLDR',7X,'ETAK',7X,'XIK',7X,'XPD',7X,'YPD
     1',7X,'XNC',7X,'YNC')
   25 FORMAT('      ')
  777 FORMAT(3F20.6)
  200 FORMAT(3F10.4)
  100 FORMAT(4I3)
  110 FORMAT(2F10.5)
  500 FORMAT(6A8)
      REAL*8 ITITLE, KTITLE, LTITLE,MTITLE
      REAL*4  LABEL/4H    /
      DIMENSION X(100),Y(100),ITITLE(12),KTITLE(12),LTITLE(12),CPG(50),
     1CPF(50),VNE(50),MTITLE(12)
      READ(5,500) (ITITLE(I),I=1,12)
      READ(5,500) (KTITLE(I),I=1,12)
      READ(5,500) (LTITLE(I),I=1,12)
      READ(5,500) (MTITLE(I),I=1,12)
      PI=3.14159
READING PARAMETERS
ALPHA IS NOZZLE TILT ANGLE
BETA IS THE PLATE ANGLE
      READ(5,110) BETA,ALPHA
EMOD IS THE MODULUS OF THE COMPLETE ELLIPTIC INTEGRAL OF THE FIRST KIND
DLDR IS THE RATIO OF DEFLECTED FLOW TO THE RIGHT AND LEFT
ETAK IS THE RATIO OF ETA SUB F TO ELP
```

```
XIK IS THE RATIO OF XI SUB A TO EL
      READ(5,7) EMOD,DLDR,ETAK,XIK
KS IS THE NUMBER OF STREAMLINE DATA POINTS
KG IS THE NUMBER OF DATA POINTS ON THE GROUND
KP IS THE NUMBER OF DATA POINTS ON THE PLATE
KV IS THE NUMBER OF DATA POINTS IN THE NOZZLE EXIT
      READ(5,100) KS,KG,KP,KV
VX IS THE MAXIMUM VOLTAGE RECORDED FOR THIS TEST
VZ IS THE VOLTAGE CORRESPONDING TO ZERO VELOCITY
SLP IS THE SLOPE OF THE CALIBRATION CURVE FOR THE HOT-WIRE PROBE
      READ(5,200) VX,VZ,SLP
VSL IS THE FREE STREAMLINE (MAXIMUM) VELOCITY
      VSL=((VX**2-VZ**2)/SLP)**2
      WRITE(6,1) VSL
CEL1 CALCULATES THE COMPLETE ELLIPTIC INTEGRAL OF THE FIRST KIND
      CALL CEL1(RES,EMOD,IER)
EL IS THE COMPLETE ELLIPTIC INTEGRAL OF THE FIRST KIND
      EL=RES
EMOP IS THE COMPLIMENTARY MODULUS
      EMOP=SQRT(1.-EMOD**2)
      CALL CEL1 (RES,EMOP,IER)
ELP IS THE COMPLETE INTEGRAL USING EMOP
      ELP=RES
SMQ IS DEFINED IN EQN B16---5064
      SMQ=EXP(-PI/2.*ELP/EL)
ETAF IS ETA SUB F
      ETAF=ETAK*ELP
XIA IS XI SUB A
      XIA=XIK*EL
JELF CALCULATES THE THREE JACOBIAN ELLIPTIC FUNCTIONS
      SCK=EMOD**2
      CALL JELF(SN,CN,DN,ETAF,SCK)
SNF, DNF, AND CNF ARE THE SN, DN, AND CN OF ETAF
      SNF=SN
      DNF=DN
      CNF=CN
SNH IS THE SN OF XI SUB H
EQN 14---5288
      SNH=(DNF/DLDR-EMOD*SNF)/(EMOD/DLDR+EMOD*SNF)
FCT IS EQN 78---5064.  IT DEFINES THE INVERSE SN
      CALL QT9A (0,SNH,FCT,EMOD,R)
XIH IS XI SUB H
      XIH=R
XIG IS XI SUB G
EQN 3---5288 (MODIFIED FOR NOZZLE TILTING)
      XIG=EL+(4.*EL/PI)*(ALPHA+BETA/2.)-2.*XIH-2.*BETA*XIA/PI
BIGM IS INTEGRAND OF EQN 18---5288
      CALL QT9B(-EL,EL,BIGM,R4,EL,ELP,EMOD,SNH,XIH,XIA,XIG,DNF,BETA,PI,R
```

```
     1)
EM IS M IN 5288
EQN 18---5288
      EM=1./(EMOP*R/PI)
VIVO IS VI/VO
EQN 18---5288
      VIVO=(1.+1./DLDR)/(SNF+1./DLDR)*EM
DR IS THE WIDTH OF THE FLOW TO THE RIGHT
EQN 12---5288
      DR=VIVO*EMOD*(1.+SNH)*SNF/(EMOD+DNF-EMOD*(1 +SNH)*(1.-SNF))
DL IS THE WIDTH OF THE FLOW TO THE LEFT
      DL=DLDR*DR
COMPUTING FUSELAGE HEIGHT AND WIDTH
ALL DISTANCES ARE NONDIMENSIONALIZED WITH NOZZLE WIDTH
BIGYP IS INTEGRAND OF EQN A6---5288
      CALL QT9B(XIG,XIA,BIGYP,R1,EL,ELP,EMOD,SNH,XIH,XIA,XIG,DNF,BETA,PI
     1,R)
YPD IS THE NONDIMENSIONAL PLATE HEIGHT
      YPD=-EM*EMOD*EMOP*R/PI
BIGXP IS INTEGRAND OF FIRST EQN A5---5288
      CALL QT9C (XIA,EL,BIGXP,BIGYP,R1,EL,ELP,EMOD,SNH,XIH,XIA,XIG,DNF,B
     1ETA,PI,R)
XPD IS NONDIMENSIONAL PLATE WIDTH
      XPD=-EM*EMOD*EMOP*R/PI
YBD AND XBD LOCATE THE POINT B
      XBD=XPD*SIN(BETA)
      YBD=YPD+XPD*COS(BETA)
NOW FIXING HORIZONTAL NOZZLE POSITION
BFX IS THE INTEGRAND OF FIRST EQN A12---5288
      CALL QT9C(0.,ELP,BFX,ACH,T4,EL,SMQ,EMOD,SNH,XIH,XIA,XIG,ETAF,BETA
     1,ALPHA,R)
      XB=R
T3 AND T4 ARE FROM EQN A7---5288 (MODIFIED FOR TILTED NOZZLES)
      THETA=T4(ETAF,BETA,XIA,XIG,XIH,SMQ,PI,EL,ALPHA)
XBXC IS THE SEPARATION OF POINTS B AND C
EQN A10---5288
  222 XBXC=EMOP**2*EM/PI*XB-DL*SIN(THETA)
XNC IS ONE HALF OF THE NOZZLE SPACING
      XNC=XBD-XBXC
NOW FIXING THE VERTICAL NOZZLE POSITION
YE IS THE INTEGRAND OF SECOND EQN A9---5288
      CALL QT9C(0.,ELP,YE,ACH,T3,EL,SMQ,EMOD,SNH,XIH,XIA,XIG,ETAF,BETA,
     1ALPHA,R)
YEYD IS THE SEPARATION OF POINTS E AND D
SECOND OF EQNS A9---5288
      YEYD=-EMOP**2*EM/PI*R
YND IS THE HEIGHT OF POINT D
      YND=DR-YEYD
```

```
YNC IS THE HEIGHT OF POINT C
      YNC=YND-SIN(ALPHA)
      WRITE(6,25)
      WRITE(6,2) BETA, ALPHA
      WRITE(6,8)
      WRITE(6,3) EMOD,DLDR,ETAK,XIK,XPD,YPD,XNC,YNC
READING STREAMLINE COORDINATES FROM DATA
      DO 101 J=1,KS
      READ(5,110) X(J),Y(J)
NONDIMENSIONALIZING COORDINATES FOR TWO INCH NOZZLES
      X(J)=X(J)/2.
      Y(J)=Y(J)/2.
  101 WRITE(6,110) X(J),Y(J)
PLOTTING FREE STREAMLINES FROM DATA
      CALL DRAW(KS,X,Y,1,5,LABEL,ITITLE,1.,1.,0,0,2,2,5,5,1,LAST)
COMPUTING FREE STREAMLINES
      ETA=ETAF+.001
COORDINATES FOR DRAWING PLATE
      X(20)=0.
      Y(20)=YPD
      X(19)=XBD
      Y(19)=YBD
COORDINATES OF STREAMLINE BF
      DO 99 J=1,18
      CALLQT9C(ETA,ELP,BFX,ACH,T4,EL,SMQ,EMOD,SNH,XIH,XIA,XIG,ETAF,BETA,
     1ALPHA,R)
      X(J)=XBD-EMOP**2*EM*R/PI
BFY IS INTEGRAND OF SECOND EQN A11---5288
      CALL QT9C(ETA,ELP,BFY,ACH,T4,EL,SMQ,EMOD,SNH,XIH,XIA,XIG,ETAF,BETA
     1,ALPHA,R)
      Y(J)=YBD+EMOP**2*EM*R/PI
      WRITE(6,777) ETA,X(J),Y(J)
   99 ETA=ETA+(ELP-ETAF)/18.
NOW PLOTTING STREAMLINE BF
      CALL DRAW(20,X,Y,2,0,LABEL,ITITLE,1.,1.,0,0,2,2,5,5,1,LAST)
      ETA=ELP/18.
COORDINATES FOR DRAWING THE NOZZLE EXIT
      X(1)=XNC
      Y(1)=YNC
      X(2)=X(1)+CCS(ALPHA)
      Y(2)=YND
COORDINATES OF STREAMLINE DE FROM EQN A9---5288
      DO 89 J=3,20
DE IS FIRST EQN A9---5288
      CALL QT9C(0.,ETA,DE,ACH,T3,EL,SMQ,EMOD,SNH,XIH,XIA,XIG,ETAF,BETA,
     1ALPHA,R)
      X(J)=X(2)+EMOP**2*EM*R/PI
      CALL QT9C(0.,ETA,YE,ACH,T3,EL,SMQ,EMOD,SNH,XIH,XIA,XIG,ETAF,BETA,
```

```
     1ALPHA,R)
      Y(J)=YND-EMCP**2*EM/PI*R
      WRITE(6,777) ETA,X(J),Y(J)
   89 ETA=ETA+ELP/18.
NOW PLOTTING STREAMLINE DE
      CALL DRAW(20,X,Y,2,0,LABEL,ITITLE,1.,1.,0,0,2,2,5,5,1,LAST)
      ETA=ETAF/20.
COMPUTING STREAMLINE COORDINATES FOR CF
      DO 79 J=1,20
      CALL QT9C(0.,ETA,BFX,ACH,T4,EL,SMQ,EMOD,SNH,XIH,XIA,XIG,ETAF,BETA,
     1ALPHA,R)
      X(J)=XNC+EMCP**2*EM*R/PI
      CALL QT9C(0.,ETA,BFY,ACH,T4,EL,SMQ,EMOD,SNH,XIH,XIA,XIG,ETAF,BETA,
     1ALPHA,R)
      Y(J)=YNC-EMCP**2*EM/PI*R
      WRITE(6,777) ETA,X(J),Y(J)
   79 ETA=ETA+ETAF/20.
PLOTTING STREAMLINE CF
      CALL DRAW(20,X,Y,3,0,LABEL,ITITLE,1.,1.,0,0,2,2,5,5,1,LAST)
READING HOT-WIRE DATA ALONG GROUND
      DO 102 J=1,KG
      READ(5,110) X(J),VOLT
      X(J)= X(J)/2.
U IS THE VELOCITY DEFINED BY EQN A4---5288
      U=(((VOLT**2-VZ**2)/SLP)**2)/VSL
CPG IS THE PRESSURE COEFFICIENT ALONG THE GROUND
      CPG(J)=1.-U**2
  102 WRITE(6,110) X(J),CPG(J)
PLOTTING PRESSURE COEFFICIENT ALONG THE GROUND
      CALL DRAW(KG,X,CPG,1,5,LABEL,KTITLE,1.,.3,0,0,2,2,5,5,1,LAST)
READING PRESSURE DATA ALONG GROUND
      DO 409  KK=1,11
      READ(5,110) X(KK),HEAD
      X(KK)=X(KK)/2.
      CPG(KK)=4758.3*HEAD/(VSL**2)
  409 WRITE(6,110) X(KK),CPG(KK)
PLOTTING PRESSURE COEFFICIENT ALONG THE GROUND
      CALL DRAW(11,X,CPG,2,2,LABEL,KTITLE,1.,.3,0,0,2,2,5,5,1,LAST)
      XI=XIG
COMPUTING THEORETICAL PRESSURE COEFFICIENT ALONG THE GROUND
      DO 69 J=1,20
      CALL QT9B(XIG,XI ,BIGYP,R1,EL,ELP,EMOD,SNH,XIH,XIA,XIG,DNF,BETA,PI
     1,R)
      X(J)=R*EM*EMOD*EMOP/PI
      U=R1(XI,XIH,EL,ELP,PI)*SQRT(ABS(R1(XI,XIG,EL,ELP,PI)))*ABS(R1(XI,X
     1IA,EL,ELP,PI))**(BETA/PI)
      CPG(J)=1.-U**2
      WRITE(6,777) XI,X(J),CPG(J)
```

```
   69 XI=XI-(XIG+EL)/20.
PLOTTING PRESSURE COEFFICIENT ALONG GROUND
      CALL DRAW(20,X,CPG,3,0,LABEL,KTITLE,1.,.3,0,0,2,2,5,5,1,LAST)
READING HOT-WIRE DATA ALONG FUSELAGE
      DO 103 J=1,KP
      READ(5,110) X(J),VOLT
      X(J)=X(J)/2.
ZETA IS THE VELOCITY DEFINED BY EQN A5---5288
      ZETA=(((VOLT**2-VZ**2)/SLP)**2)/VSL
CPF IS THE PRESSURE COEFFICIENT ALONG THE FUSELAGE
      CPF(J)=1.-ZETA**2
  103 WRITE(6,110) X(J),CPF(J)
PLOTTING PRESSURE COEFFICIENT ALONG THE FUSELAGE
      CALL DRAW(KP,X,CPF,1,5,LABEL,LTITLE,.3,.3,0,0.2,2,5,5,1,LAST)
      XI=XIA
COMPUTING THEORETICAL PRESSURE COEFFICIENT ALONG THE FUSELAGE
      DO 59 J=1,20
      CALL QT9B(XIA,XI ,BIGYP,R1,EL,ELP,EMOD,SNH,XIH,XIA,XIG,DNF,BETA,PI
     1,R)
      X(J)=-R*EM*EMOD*EMOP/PI
      ZETA=-R1(XI,XIH,EL,ELP,PI)*SQRT(ABS(R1(XI,XIG,EL,ELP,PI)))*ABS(R1(
     1XI,XIA,EL,ELP,PI))**(BETA/PI)
      CPF(J)=1.-ZETA**2
      WRITE(6,777) XI,X(J),CPF(J)
   59 XI=XI+(EL-XIA)/20.
PLOTTING THE PRESSURE COEFFICIENT ALONG THE FUSELAGE
      CALL DRAW(20,X,CPF,3,0,LABEL,LTITLE,.3,.3,0,0,2,2,5,5,1,LAST)
READING VELOCITY DATA IN NOZZLE EXIT
      DO 104 J=1,KV
      READ(5,110) X(J),VOLT
      X(J)=X(J)/2.
VNE IS THE RATIO OF NOZZLE VELOCITY TO FREE STREAM VELOCITY
      VNE(J)=  -(((VOLT**2-VZ**2)/SLP)**2)/VSL
  104 WRITE(6,110) X(J),VNE(J)
PLOTTING VELOCITY PROFILE IN THE NOZZLE EXIT
      CALL DRAW(KV,X,VNE,1,5,LABEL,MTITLE,.2,.2,5,0,2,2,5,5,1,LAST)
      XI=-EL
COMPUTING THE THEORETICAL VELOCITY PROFILE IN THE NOZZLE EXIT
      DO 49 J=1,20
EX IS EQN A3---5288
      CALL QT9B(-EL,XI,EX,R4,EL,ELP,EMOD,SNH,XIH,XIA,XIG,DNF,BETA,PI,R)
      X(J)=1.-R*EM*EMOP/PI
      VNE(J)=R4(XI,XIH,EL,ELP,PI)*SQRT(ABS(R4(XI,XIG,EL,ELP,PI)))*ABS(R4
     1(XI,XIA,EL,ELP,PI))**(BETA/PI)
FIX VELOCITY DIRECTION DOWNWARD
      VNE(J)=-VNE(J)
      XI=XI+EL/10.
      WRITE(6,777) XI,X(J),VNE(J)
```

```
   49 CONTINUE
PLOTTING VELOCITY PROFILE IN THE NOZZLE EXIT
      CALL DRAW(20,X,VNE,3,0,LABEL,MTITLE,.2,.2,5,0,2,2,5,5,1,LAST)
      STOP
      END


      SUBROUTINE CEL1(RES,AK,IER)
TAKEN FROM COMPUTER FACILITY SUBROUTINE LIBRARY
      IER=0
      ARI=2.
      GEO=(0.5-AK)+0.5
      GEO=GEO+GEO*AK
      RES=C.5
      IF(GEO)1,2,4
    1 IER=1
    2 RES=1.E75
      RETURN
    3 GEO=GEO*AARI
    4 GEO=SQRT(GEO)
      GEO=GEO+GEO
      AARI=ARI
      ARI=ARI+GEO
      RES=RES+RES
      IF( GEO/AARI-0.9999)3,5,5
    5 RES=RES/ARI*6.283185E0
      RETURN
      END


      SUBROUTINE JELF(SN,CN,DN,X,SCK)
TAKEN FROM COMPUTER FACILITY SUBROUTINE LIBRARY
      DIMENSION ARI(12),GEO(12)
      CM=SCK
      Y=X
      IF(SCK)3,1,4
    1 D=EXP(X)
      A=1./D
      B=A+D
      CN=2./B
      DN=CN
      SN=TANH(X)
    2 RETURN
    3 D=1.-SCK
      CM=-SCK/D
      D=SQRT(D)
      Y=D*X
    4 A=1.
```

```
      DN=1.
      DO 6 I=1,12
      L=I
      ARI(I)=A
      CM=SQRT(CM)
      GEO(I)=CM
      C=(A+CM)*.5
      IF(ABS(A-CM)-1.E-4*A)7,7,5
    5 CM=A*CM
    6 A=C
    7 Y=C*Y
      SN=SIN(Y)
      CN=COS(Y)
      IF(SN)8,13,8
    8 A=CN/SN
      C=A*C
      DO 9 I=1,L
      K=L-I+1
      B=ARI(K)
      A=C*A
      C=DN*C
      DN=(GEO(K)+A)/(B+A)
    9 A=C/B
      A=1./SQRT(C*C+1.)
      IF(SN)10,11,11
   10 SN=-A
      GO TO 12
   11 SN=A
   12 CN=C*SN
   13 IF(SCK)14,2,2
   14 A=DN
      DN=CN
      CN=A
      SN=SN/D
      RETURN
      END


      SUBROUTINE GT9A (XL,XU,FCT,EMOD,R)
INTEGRATION BY GAUSS 9-POINT QUADRATURE FORMULA
      A=.5*(XU+XL)
      B=XU-XL
      C=.4840801*B
      R=.04063719*(FCT(A+C,EMOD)+FCT(A-C,EMOD))
      C=.4180156*B
      R=R+.09032408*(FCT(A+C,EMOD)+FCT(A-C,EMOD))
      C=.3066857*B
      R=R+.13030534*(FCT(A+C,EMOD)+FCT(A-C,EMOD))
```

```
      C=.1621267*B
      R=R+.1561735*(FCT(A+C,EMOD)+FCT(A-C,EMOD))
      R=B*(R+.1651197*FCT(A,EMOD))
      RETURN
      END


      SUBROUTINE QT9B(XL,XU,FCT,T,EL,EL1,EMOD,SNH,XIH,XIA,XIG,ETAF,BETA,
INTEGRATION BY GAUSS 9-POINT QUADRATURE FORMULA
     1PI,R)
      A=.5*(XU+XL)
      B=XU-XL
      C=.4840801*B
      P =FCT(A+C,T,EL,EL1,EMOD,SNH,XIH,XIA,XIG,ETAF,BETA,PI)
      PM=FCT(A-C,T,EL,EL1,EMOD,SNH,XIH,XIA,XIG,ETAF,BETA,PI)
    2 R=.04063719*(P+PM)
      C=.4180156*B
      R=R+.0903240 8*(FCT(A+C,T,EL,EL1,EMOD,SNH,XIH,XIA,XIG,ETAF,BETA,PI)
     1+FCT(A-C,T,EL,EL1,EMOD,SNH,XIH,XIA,XIG,ETAF,BETA,PI))
      C=.3066857*B
      R=R+.1303053*(FCT(A+C,T,EL,EL1,EMOD,SNH,XIH,XIA,XIG,ETAF,BETA,PI)+
     1FCT(A-C,T,EL,EL1,EMOD,SNH,XIH,XIA,XIG,ETAF,BETA,PI))
      C=.1621267*B
      R=R+.1561735*(FCT(A+C,T,EL,EL1,EMOD,SNH,XIH,XIA,XIG,ETAF,BETA,PI)+
     1FCT(A-C,T,EL,EL1,EMOD,SNH,XIH,XIA,XIG,ETAF,BETA,PI))
      R=B*(R+.1651197*FCT(A,T,EL,EL1,EMOD,SNH,XIH,XIA,XIG,ETAF,BETA,PI))
      RETURN
      END


      SUBROUTINE QT9C(XL,XU,FCT,ACH,T,EL,SMQ,EMOD,SNH,XIH,XIA,XIG,ETAF,
INTEGRATION BY GAUSS 9-POINT QUADRATURE FORMULA
     1BETA,ALPHA,R)
      A=.5*(XU+XL)
      B=XU-XL
      C=.4840801*B
      P=FCT(A+C,ACH,T,EL,SMQ,EMOD,SNH,XIH,XIA,XIG,ETAF,BETA,ALPHA)
      PM=FCT(A-C,ACH,T,EL,SMQ,EMOD,SNH,XIH,XIA,XIG,ETAF,BETA,ALPHA)
    2 R=.04063719*(P+PM)
      C=.4180156*B
      R=R+.0903240 8*(FCT(A+C,ACH,T,EL,SMQ,EMOD,SNH,XIH,XIA,XIG,ETAF,BETA
     1,ALPHA)+FCT(A-C,ACH,T,EL,SMQ,EMOD,SNH,XIH,XIA,XIG,ETAF,BETA,ALPHA
     2))
      C=.3066857*B
      R=R+.1303053*(FCT(A+C,ACH,T,EL,SMQ,EMOD,SNH,XIH,XIA,XIG,ETAF,BETA
     1,ALPHA)+FCT(A-C,ACH,T,EL,SMQ,EMOD,SNH,XIH,XIA,XIG,ETAF,BETA,ALPHA
     2))
      C=.1621267*B
```

```
      R=R+.1561735*(FCT(A+C,ACH,T,EL,SMQ,EMOD,SNH,XIH,XIA,XIG,ETAF,BETA
     1,ALPHA)+FCT(A-C,ACH,T,EL,SMQ,EMOD,SNH,XIH,XIA,XIG,ETAF,BETA,ALPHA
     2))
      R=B*(R+.1651197*FCT(A,ACH,T,EL,SMQ,EMOD,SNH,XIH,XIA,XIG,ETAF,BETA
     1,ALPHA))
      RETURN
      END


      SUBROUTINE TQ3(ETA,R,SMQ,PI,EL,Q3)
A4, A3, B4 AND B3 ARE EQN B16---5064
      A4(ETA,R,SMQ,PI,EL)=1.+2.*(-SMQ*COS(PI/(2.*EL)*(EL-R))*COSH(PI/(2
     1*EL)*ETA)+SMQ**4*COS(PI/EL*(EL-R))*COSH(PI/EL*ETA)-SMQ**9*COS(3.*P
     2I/(2.*EL)*(EL-R))*COSH(3.*PI/(2.*EL)*ETA)+SMQ**16*COS(2.*PI/EL*(EL
     3-R))*COSH(2.*PI/EL*ETA))
      B4(ETA,R,SMQ,PI,EL)=-2.*(-SMQ*SIN(PI/(2.*EL)*(EL-R))*SINH(PI/(2.*E
     1L)*ETA)+SMQ**4*SIN(PI/EL*(EL-R))*SINH(PI/EL*ETA)-SMQ**9*SIN(3.*PI/
     2(2.*EL)*(EL-R))*SINH(3.*PI/(2.*EL)*ETA)+SMQ**16*SIN(2.*PI/EL*(EL-R
     1))*SINH(2.*PI/EL*ETA))
      A3(ETA,R,SMQ,PI,EL)=4.*(SMQ*COS(PI/(2.*EL)*(EL-R))*COSH(PI/(2.*EL)
     1*ETA)+SMQ**9*COS(3.*PI/(2.*EL)*(EL-R))*COSH(3.*PI/(2.*EL)*ETA))+A4
     2(ETA,R,SMQ,PI,EL)
      B3(ETA,R,SMQ,PI,EL)=-4.*(SMQ*SIN(PI/(2.*EL)*(EL-R))*SINH(PI/(2.*EL
     1)*ETA)+SMQ**9*SIN(3.*PI/(2.*EL)*(EL-R))*SINH(3.*PI/(2.*EL)*ETA))+B
     24(ETA,R,SMQ,PI,EL)
      TOP=A3(ETA,R,SMQ,PI,EL)**2-B3(ETA,R,SMQ,PI,EL)**2
      BOT=A3(ETA,R,SMQ,PI,EL)**2+B3(ETA,R,SMQ,PI,EL)**2
      IF((ABS(TOP)-ABS(BOT)*.00001).GT.0.) GO TO 4
Q3 IS DERIVED FROM EQN B17---5064
Q3 MUST ALWAYS BE TAKEN AS A NEGATIVE ANGLE IN THE THIRD OR FOURTH QUADRANT
      Q3=-PI/2.
      RETURN
    4 Q3=ARCOS(TOP/BOT)
    3 IF(ABS(Q3)-999.9) 2,2,1
    1 Q3=Q3/(2.*PI)
      GO TO 3
    2 Q3=-ABS(Q3)
   10 IF(ABS(Q3).LE.PI) RETURN
      Q3=-Q3
   11 T=Q3/(2.*PI)
      I=T
      U=I
      Q3=(T-U)*2.*PI
      Q3=Q3-2.*PI
      RETURN
      END
```

```
      SUBROUTINE TQ4(ETA,R,SMQ,PI,EL,Q4)
A4 AND B4 ARE EQN B16---5064
      A4(ETA,R,SMQ,PI,EL)=1.+2.*(-SMQ*COS(PI/(2.*EL)*(EL-R))*COSH(PI/(2
     1*EL)*ETA)+SMQ**4*COS(PI/EL*(EL-R))*COSH(PI/EL*ETA)-SMQ**9*COS(3.*P
     2I/(2.*EL)*(EL-R))*COSH(3.*PI/(2.*EL)*ETA)+SMQ**16*COS(2.*PI/EL*(EL
     3-R))*COSH(2.*PI/EL*ETA))
      B4(ETA,R,SMQ,PI,EL)=-2.*(-SMQ*SIN(PI/(2.*EL)*(EL-R))*SINH(PI/(2.*E
     1L)*ETA)+SMQ**4*SIN(PI/EL*(EL-R))*SINH(PI/EL*ETA)-SMQ**9*SIN(3.*PI/
     2(2.*EL)*(EL-R))*SINH(3.*PI/(2.*EL)*ETA)+SMQ**16*SIN(2.*PI/EL*(EL-R
     1))*SINH(2.*PI/EL*ETA))
      TOP=A4(ETA,R,SMQ,PI,EL)**2-B4(ETA,R,SMQ,PI,EL)**2
      BOT=A4(ETA,R,SMQ,PI,EL)**2+B4(ETA,R,SMQ,PI,EL)**2
      IF((ABS(TOP)-ABS(BOT)*.00001).GT.0.) GO TO 4
Q4 IS DERIVED FROM EQN B17---5064
Q4 MUST ALWAYS BE TAKEN AS A POSITIVE ANGLE IN THE FIRST OR SECOND QUADRANT
      Q4=1.57079
      RETURN
    4 Q4=ABS(ARCOS(TOP/BOT))
    3 IF(Q4-999.9) 2,2,1
    1 Q4=Q4/(2.*PI)
      GO TO 3
    2 T=Q4/(2.*PI)
      I=T
      U=I
      Q4=(T-U)*2.*PI
      IF(Q4.GE.0..AND.Q4.LE.PI) RETURN
      X=Q4/PI
      K=X
      Y=K
      Q4=(1.-X+Y)*PI
      RETURN
      END


      FUNCTION FCT(T,EMOD)
DEFINES INVERSE SN
      FCT=1./SQRT((1.-T**2)*(1.-(EMOD*T)**2))
      RETURN
      END


      FUNCTION BIGM(XI,R4,EL,ELP,EMOD,SNH,XIH,XIA,XIG,DNF,BETA,PI)
EVALUATES INTEGRAND OF EQN 18---5288
      SCK=1.-EMOD**2
      CALL JELF(SN,CN,DN,XI,SCK)
      SNX=SN
      DNX=DN
      DEN=DNX*(1.-DNF*SNX)*R4(XI,XIH,EL,ELP,PI)*SQRT(ABS(R4(XI,XIG,EL,EL
```

```
     1P,PI)))*(ABS(R4(XI,XIA,EL,ELP,PI)))**(BETA/PI)
    2 BIGM=((1.-EMOD*SNH*SNX)*(1.-EMOD*SNX))/DEN
      RETURN
      END


      FUNCTION ACH(I,ETA,SNH,ETAF,EMOD)
ACH IS EQN A8---5288
WHEN I=1 ACH CALCULATES H+
WHEN I=2 ACH CALCULATES H-
      EMOP=SQRT(1.-EMOD**2)
      SCK=1.-EMOP**2
      CALL JELF(SN,CN,DN,ETA,SCK)
      CNE=CN
      DNE=DN
      CALL JELF(SN,CN,DN,ETAF,SCK)
      DNF=DN
      IF(I-1)10,10,11
   10 DEN=(DNE-EMOD)*(DNE+DNF)
    9 ACH=(DNE+EMOD*SNH)*CNE/DEN
      GO TO 12
   11 DEN=(DNE+EMOD)*(DNE-DNF)
   14 ACH=(DNE-EMOD*SNH)*CNE/DEN
   12 RETURN
      END


      FUNCTION R1(XI,R,EL,ELP,PI)
R1 IS EQN B3---5064
TH1 IS THE FIRST THETA FUNCTION
      COMPLEX*8 TH1,Z,TA
      TH1(Z,PI,TA)=2.*(CEXP((0.,1.)*PI*TA*0.25)*CSIN(Z)-CEXP((0.,1.)*PI*
     1TA*1.5**2)*CSIN(3.*Z)+CEXP((0.,1.)*PI*TA*2.5**2)*CSIN(5.*Z)-CEXP((
     20.,1.)*PI*TA*3.5**2)*CSIN(7.*Z)+CEXP((0.,1.)*PI*TA*4.5**2)*CSIN(9.
     3*Z)-CEXP((0.,1.)*PI*TA*5.5**2)*CSIN(11.*Z))
      R1=TH1((1.,0.)*PI/(4.*EL)*(R-XI),PI,(0.,1.)*ELP/(2.*EL))/TH1((1.,0
     1.)*PI/(4.*EL)*(2.*EL-XI-R),PI,(0.,1.)*ELP/(2.*EL))
      RETURN
      END


      FUNCTION R4(XI,R,EL,ELP,PI)
R4 IS EQN B2---5064
TH4 IS THE FOURTH THETA FUNCTION
      COMPLEX*8 TH4,Z,TA
      TH4(Z,PI,TA)=(1.,0.)+(2.,0.)*(-CEXP((0.,1.)*PI*TA)*CCOS(2.*Z)+CEXP
     1((0.,4.)*PI*TA)*CCOS(4.*Z)-CEXP((0.,9.)*PI*TA)*CCOS(6.*Z)+CEXP((0.,
     2,16.)*PI*TA)*CCOS(8.*Z))
```

```
      R4=TH4((1.,0.)*PI/(4.*EL)*(R-XI),PI,(0.,1.)*ELP/(2.*EL))/TH4((1.,0
     1.)*PI/(4.*EL)*(2.*EL-XI-R),PI,(0.,1.)*ELP/(2.*EL))
      RETURN
      END


      FUNCTION T3(ETA,BETA,A,G,H,SMQ,PI,EL,ALPHA)
EVALUATES EQN A7---5288 FOR I=3
      CALL TQ3(ETA,H,SMQ,PI,EL,Q3)
      Q3H=Q3
      CALL TQ3(ETA,A,SMQ,PI,EL,Q3)
      Q3A=Q3
      CALL TQ3(ETA,G,SMQ,PI,EL,Q3)
      Q3G=Q3
      T3=PI/2.+Q3H+Q3G/2.+BETA*Q3A/PI-ALPHA
      RETURN
      END


      FUNCTION T4(ETA,BETA,A,G,H,SMQ,PI,EL,ALPHA)
EVALUATES EQN A7---5288 FOR I=4
      CALL TQ4(ETA,H,SMQ,PI,EL,Q4)
      Q4H=Q4
      CALL TQ4(ETA,G,SMQ,PI,EL,Q4)
      Q4G=Q4
      CALL TQ4(ETA,A,SMQ,PI,EL,Q4)
      Q4A=Q4
      T4=PI/2.+Q4H+Q4G/2.+BETA*Q4A/PI-ALPHA
      RETURN
      END


      FUNCTION BIGYP(XI,R1,EL,ELP,EMOD,SNH,XIH,XIA,XIG,DNF,BETA,PI)
EVALUATES INTEGRAND OF EQN A6---5288
      SCK=1.-EMOD**2
      CALL JELF(SN,CN,DN,XI,SCK)
      DEN=CN*(DNF-EMOD*SN)*R1(XI,XIH,EL,ELP,PI)*SQRT(ABS(R1(XI,XIG,EL,EL
     1P,PI)))*(ABS(R1(XI,XIA,EL,ELP,PI)))**(BETA/PI)
CHECK FOR ZERO DENOMINATOR
      IF(ABS(DEN)-.00001)13,13,3
   13 BIGYP=1000.
      RETURN
    3 BIGYP=((SN-SNH)*(1.-SN))/DEN
      RETURN
      END
```

```
      FUNCTION BIGXP(XI,BIGYP,R1,EL,ELP,EMOD,SNH,XIH,XIA,XIG,DNF,BETA,
     1PI)
EVALUATES INTEGRAND OF EQN A5---5288
      BIGXP=BIGYP(XI,R1,EL,ELP,EMOD,SNH,XIH,XIA,XIG,DNF,BETA,PI)
      RETURN
      END

      FUNCTION DE(ETA,ACH,T3,EL,SMQ,EMOD,SNH,XIH,XIA,XIG,ETAF,BETA,ALPHA
     1)
EVALUATES INTEGRAND OF FIRST EQN A9---5288
      PI=3.14159
      THETA=T3(ETA,BETA,XIA,XIG,XIH,SMQ,PI,EL,ALPHA)
    1 DE=ACH(1,ETA,SNH,ETAF,EMOD)*COS(THETA)
      RETURN
      END

      FUNCTION YE(ETA,ACH,T3,EL,SMQ,EMOD,SNH,XIH,XIA,XIG,ETAF,BETA,ALPHA
     1)
EVALUATES INTEGRAND OF SECOND EQN A9---5288
      PI=3.14159
      THETA=T3(ETA,BETA,XIA,XIG,XIH,SMQ,PI,EL,ALPHA)
    1 YE=ACH(1,ETA,SNH,ETAF,EMOD)*SIN(THETA)
      RETURN
      END

      FUNCTION BFX(ETA,ACH,T4,EL,SMQ,EMOD,SNH,XIH,XIA,XIG,ETAF,BETA,
     1ALPHA)
EVALUATES INTEGRAND OF FIRST EQN A12---5288
      PI=3.14159
      THETA=T4(ETA,BETA,XIA,XIG,XIH,SMQ,PI,EL,ALPHA)
    1 BFX=ACH(2,ETA,SNH,ETAF,EMOD)*COS(THETA)
      RETURN
      END

      FUNCTION BFY(ETA,ACH,T4,EL,SMQ,EMOD,SNH,XIH,XIA,XIG,ETAF,BETA,
     1ALPHA)
EVALUATES INTEGRAND OF SECOND EQN A12---5288
      PI=3.14159
      THETA=T4(ETA,BETA,XIA,XIG,XIH,SMQ,PI,EL,ALPHA)
    1 BFY=ACH(2,ETA,SNH,ETAF,EMOD)*SIN(THETA)
      RETURN
      END
```

```
      FUNCTION EX(XI,R4,EL,ELP,EMOD,SNH,XIH,XIA,XIG,DNF,BETA,PI)
EVALUATES INTEGRAND OF EQN A3---5288
      SCK=1.-EMOD**2
      CALL JELF(SN,CN,DN,XI,SCK)
      DEN=DN*(1.-DNF*SN)*R4(XI,XIH,EL,ELP,PI)*SQRT(ABS(R4(XI,XIG,EL,ELP,
     1PI)))*(ABS(R4(XI,XIA,EL,ELP,PI)))**(BETA/PI)
CHECK FOR ZERO DENOMINATOR
      IF(ABS(DEN)-.00001)13,13,3
   13 EX=1000.
      RETURN
    3 EX=((1.-EMOD*SNH*SN)*(1.-EMOD*SN))/DEN
      RETURN
      END
```

BIBLIOGRAPHY

1. Campbell, John Paul, Vertical Takeoff and Landing Aircraft, The Macmillan Co., New York, 1962.

2. Gedney, Richard T. and Siegel, Robert, Inviscid Flow Analysis of Two Parallel Slot Jets Impinging Normally on a Surface, NASA TN D-4957, 1968.

3. Goldstein, Marvin E. and Siegel, Robert, Analysis of Two Dimensional Inviscid Model of Jet Impingment Under Vertical-Takeoff Airplane, NASA TN D-5288, 1969.

4. Goldstein, Marvin E. and Siegel, Robert, Two Dimensional Inviscid Jet Flow from Two Nozzles at an Angle to a Plane Surface, NASA TN D-5064, 1969.

5. Moretti, Gino, Functions of a Complex Variable, Prentice-Hall, Inc., 1964.

6. North Atlantic Treaty Organization Advisory Group for Aeronautical Research and Development, Symposium on Vertical/Short Takeoff and Landing Aircraft, Proceedings, 1960.

7. Rainville, Earl D., Special Functions, The Macmillan Co., New York, 1960.

8. Whittaker, Edmund T., and Watson, G. N., A Course of Modern Analysis, Fourth Edition, Cambridge Univ. Press, 1927.

INITIAL DISTRIBUTION LIST

		No. Copies
1.	Defense Documentation Center Cameron Station Alexandria, Virginia 22314	2
2.	Library, Code 0212 Naval Postgraduate School Monterey, California 93940	2
3.	Assistant Professor T. M. Houlihan, Code 59Hm Department of Mechanical Engineering Naval Postgraduate School Monterey, California 93940	1
4.	LTJG Charles Douglas Thompson, USN 334 South Worthington West Memphis, Arkansas 72301	1
5.	Professor T. Sarpkaya, Code 59Sl Department of Mechanical Engineering Naval Postgraduate School Monterey, California 93940	1
6.	Assistant Professor R. H. Nunn, Code 59Nn Department of Mechanical Engineering Naval Postgraduate School Monterey, California 93940	1
7.	Dr. Marvin E. Goldstein Lewis Research Center National Aeronautics and Space Administration Cleveland, Ohio 129-01-07-07-22	1

Security Classification

DOCUMENT CONTROL DATA - R & D

(Security classification of title, body of abstract and indexing annotation must be entered when the overall report is classified)

ORIGINATING ACTIVITY *(Corporate author)*

Naval Postgraduate School
Monterey, California 93940

2a. REPORT SECURITY CLASSIFICATION

Unclassified

2b. GROUP

REPORT TITLE

An Investigation of Ground Effect on Vertical Takeoff Aircraft

DESCRIPTIVE NOTES *(Type of report and, inclusive dates)*

Master's Thesis; June 1970

AUTHOR(S) *(First name, middle initial, last name)*

Charles Douglas Thompson

REPORT DATE	7a. TOTAL NO. OF PAGES	7b. NO. OF REFS
June 1970	74	8

CONTRACT OR GRANT NO.

PROJECT NO.

9a. ORIGINATOR'S REPORT NUMBER(S)

9b. OTHER REPORT NO(S) *(Any other numbers that may be assigned this report)*

DISTRIBUTION STATEMENT

This document has been approved for public release and sale;
its distribution is unlimited.

SUPPLEMENTARY NOTES

12. SPONSORING MILITARY ACTIVITY

Naval Postgraduate School
Monterey, California 93940

ABSTRACT

The theoretical solution for the flow beneath V/STOL aircraft was extended to include tilted jet configurations. A laboratory model was constructed to test the effect of variation of the parameters governing the flow. Free streamline plots, pressure coefficients on the ground and fuselage and velocity profiles in the nozzles were determined from hot-wire anemometer traverses and micromanometer readings. Experimental data compared favorably with the theoretical determinations.

D FORM 1 NOV 65 1473 (PAGE 1)

N 0101-807-6811

Security Classification

A-31408

KEY WORDS	LINK A		LINK B		LINK C	
	ROLE	WT	ROLE	WT	ROLE	WT
Ground effect						
Vertical Takeoff Aircraft						

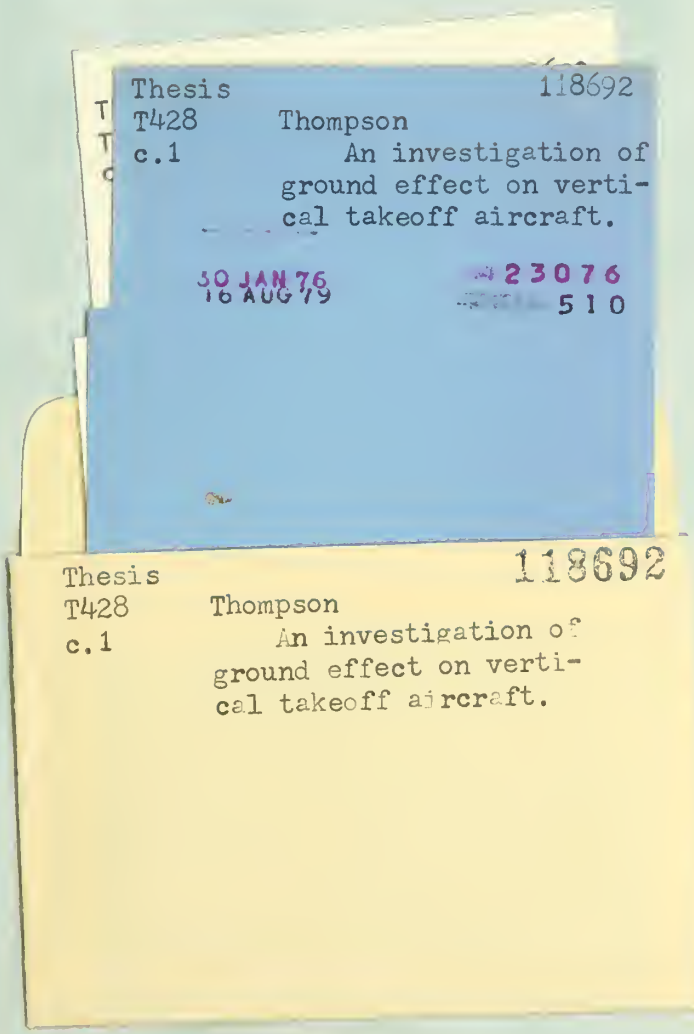

Thesis 118692
T428 Thompson
c.1 An investigation of ground effect on vertical takeoff aircraft.